The *Listeria monocytogenes* persistence factor ClpL is a potent stand-alone disaggregase

Valentin Bohl[1], Nele Merret Hollmann[2], Tobias Melzer[1], Panagiotis Katikaridis[1], Lena Meins[1], Bernd Simon[2], Dirk Flemming[3], Irmgard Sinning[3], Janosch Hennig[2,4] and Axel Mogk[1*]

[1] Center for Molecular Biology of Heidelberg University (ZMBH), DKFZ-ZMBH Alliance, Im Neuenheimer Feld 282, 69120 Heidelberg, Germany

[2] Structural and Computational Biology Unit, European Molecular Biology Laboratory (EMBL) Heidelberg, Meyerhofstrasse 1, 69117 Heidelberg, Germany

[3] Heidelberg University Biochemistry Center (BZH), Im Neuenheimer Feld 328, 69120 Heidelberg, Germany

[4] Chair of Biochemistry IV, Biophysical Chemistry, University of Bayreuth, Universitätsstrasse 30, 95447 Bayreuth, Germany

* Corresponding author: Axel Mogk
Email: a.mogk@zmbh.uni-heidelberg.de

Running title: Autonomous ClpL disaggregase confers extreme heat resistance

Keywords: ATPase associated with diverse cellular activities (AAA), protein aggregation, molecular chaperone, heat resistance,

Abstract

Heat stress can cause cell death by triggering the aggregation of essential proteins. In bacteria, aggregated proteins are rescued by the canonical Hsp70/AAA+ (ClpB) bi-chaperone disaggregase. Man-made, severe stress conditions applied during e.g. food-processing represent a novel threat for bacteria by exceeding the capacity of the Hsp70/ClpB system. Here, we report on the potent autonomous AAA+ disaggregase ClpL from *Listeria monocytogenes* that provides enhanced heat resistance to the food-borne pathogen enabling persistence in adverse environments. ClpL shows increased thermal stability and enhanced disaggregation power compared to Hsp70/ClpB, enabling it to withstand severe heat stress and to solubilize tight aggregates. ClpL binds to protein aggregates via aromatic residues present in its N-terminal domain (NTD) that adopts a partially folded and dynamic conformation. Target specificity is achieved by simultaneous interactions of multiple NTDs with the aggregate surface. ClpL shows remarkable structural plasticity by forming diverse higher assembly states through interacting ClpL rings. NTDs become largely sequestered upon ClpL ring interactions. Stabilizing ring assemblies by engineered disulfide bonds strongly reduces disaggregation activity, suggesting that they represent storage states.

Introduction

Listeria monocytogenes (*Lm*) is a food-borne pathogen and the causative agent of listeriosis, a severe human illness that is acquired upon eating contaminated food with a mortality of 20-30 % (Bucur *et al*, 2018). While *Lm* can efficiently persist in food-producing plants it cannot grow at temperatures above 45°C, qualifying heat treatments as efficient possibility to eradicate the pathogen. However, *Lm* strains that show an up to 1000-fold enhanced heat resistance have been described (Lunden *et al*, 2008). Environmental and food-related *Lm* strains frequently harbor plasmids that encode for open reading frames providing protection against antibiotics, disinfectants, heavy metals, high salt concentrations, low pH and heat stress (Jiang *et al*, 2016; Lebrun *et al*, 1994; Naditz *et al*, 2019; Pontinen *et al*, 2017; Poyart-Salmeron *et al*, 1990). Heat resistance at 55°C is provided by the chaperone ClpL, which is encoded on diverse *Lm* plasmids (Pontinen *et al.*, 2017). ClpL presence does not increase the maximum growth temperature of *L. monocytogenes* but strongly enhances cell survival upon sudden exposure to extreme temperatures. ClpL is also encoded in the core genome of various Gram-positive bacteria including the major pathogens *Staphylococcus aureus* and *Streptococcus pneumoniae*. *clpL* gene expression is typically upregulated upon heat shock and *clpL* knockout strains can exhibit increased sensitivity to heat stress suggesting a function of ClpL in cellular proteostasis (Li *et al*, 2011; Suokko *et al*, 2008; Suokko *et al*, 2005).

ClpL belongs to the AAA+ (ATPase associated with diverse cellular activities) protein family. AAA+ proteins typically form hexameric assemblies and thread substrates through an inner channel under consumption of ATP. This threading activity of AAA+ proteins is linked to unfolding and disassembly of substrates (Puchades *et al*, 2020). *In vitro* ClpL, originating from other Gram-positive bacteria, was shown to exhibit chaperone activity, however, which specific role ClpL plays in bacterial proteostasis remained undefined (Kwon *et al*, 2003; Park *et al*, 2015; Tao & Biswas, 2013).

Severe heat shock triggers massive protein aggregation, titrating crucial components of essential cellular processes including transcription, translation and cell division. Cells are therefore equipped with protein disaggregases that rescue aggregated proteins and protect cells from the deleterious consequences of protein aggregation. In bacteria the AAA+ protein ClpB cooperates with the Hsp70 (DnaK) chaperone to form the canonical and widespread bi-chaperone disaggregation system (Mogk *et al*, 1999; Zolkiewski, 1999). Notably, ClpB does not directly bind to protein aggregates but requires Hsp70 for aggregate targeting (Winkler *et al*, 2012). The DnaK/ClpB disaggregation activity is well adapted to temperature gradients, which allow for increasing disaggregation capacity through induction of stress responses. Surprisingly, ClpB is equipped with a reduced unfolding power (Haslberger *et al*, 2008), limiting its disaggregation efficiency *in vitro* towards tight aggregates forming at high unfolding temperatures (Katikaridis *et al*, 2019).

Bacteria face new stress conditions in the industrial world including abrupt temperature jumps applied during e.g. food-processing to reduce the number of bacterial contaminants. Selected Gram-negative bacteria including major pathogens like *Pseudomonas aeruginosa* (*Pa*) or *Klebsiella pneumoniae* adapt to these man-made stress regimes by acquiring the autonomous AAA+ ClpG disaggregase, which confers extreme heat resistance (Bojer *et al*, 2010; Boll *et al*, 2017; Lee *et al*, 2018). *clpG* is encoded on plasmids or mobile genomic islands (tLST: transmissible locus of stress resistance) together with other open reading frames linked to protein quality control (Kamal *et al*, 2021b). The tLST cluster can be transferred to other bacteria via horizontal gene transfer. ClpG homologs are not present in Gram-positive bacteria and a disaggregase counterpart sharing mechanistic features has not been described yet. The characteristics of *Lm* ClpL, including its link to superior heat resistance and its presence on conjugative plasmids (Pontinen *et al.*, 2017), show remarkable similarity to ClpG.

Here, we characterize *Lm* ClpL as autonomous and general, robust disaggregase. This defines ClpL as counterpart of ClpG in Gram-positive bacteria. ClpL has higher disaggregation activity

as compared to the canonical *Lm* DnaK/ClpB disaggregase by applying enhanced threading forces. Furthermore, ClpL shows increased thermostability compared to *Lm* DnaK, enabling it to withstand more severe heat stress conditions. ClpL achieves aggregate specificity via a unique N-terminal domain (NTD), which features mobile secondary structure elements and interacts with protein aggregates via patches of aromatic residues. The comparison of ClpL and ClpG allows to define mechanistic features shared by stand-alone bacterial disaggregases.

Results

L. monocytogenes ClpL is an autonomous disaggregase

Lm ClpL increases heat resistance and is encoded on conjugative plasmids, thus sharing characteristic features with the autonomous, potent disaggregase ClpG from selected Gram-negative bacteria. ClpL also has a similar domain organization as compared to the stand-alone *Pa* ClpG and the Hsp70-dependent ClpB disaggregase, including two AAA domains, a coiled-coil M-domain (MD) and the absence of a ClpP interaction motif, implying a function independent of protein degradation (Figure 1A, Figure 1 – figure supplement 1). We therefore asked whether ClpL represents a stand-alone disaggregase, functioning as counterpart of ClpG in Gram-positive bacteria. ClpL showed substantial disaggregation activity towards heat-aggregated Luciferase that was 0.67-fold reduced as compared to ClpG, but 3.1-fold higher as compared to the *Lm* Hsp70 (KJE)-ClpB bi-chaperone disaggregase, which we included as references (Figure 1B). Addition of *Lm* KJE to ClpL increased the reactivation of aggregated Luciferase 1.7-fold, however, it did hardly enhance ClpL disaggregation activity when monitored directly by turbidity measurements (Figure 1 -figure supplement 2A/B). This argues against a direct cooperation of *Lm* ClpL and KJE in disaggregation and points to a role of *Lm* KJE in supporting refolding of disaggregated Luciferase.

We next tested whether ClpL acts as a general, robust disaggregase by monitoring disaggregation of other heat aggregated model substrates: GFP, α-Glucosidase and Malate Dehydrogenase (MDH). ClpL always showed high disaggregation activity that was similar to *Pa* ClpG and vastly superior to *Lm* KJE/ClpB (Figure 1C, Figure 1 – figure supplement 2C/D). Combining ClpL with *Lm* KJE always led to a strong reduction in disaggregation activity, which can be explained by competition for protein aggregate binding, as observed for ClpG before (Lee *et al.*, 2018). We also compared *Lm* ClpL disaggregation activity with the *E. coli* (*Ec*) KJE/ClpB system, documenting similar (Luciferase, MDH) or approx. 2.5-fold enhanced (GFP, α-Glucosidase) activities (Figure 1 – figure supplement 2E). Addition of *Ec* KJE to ClpL reduced or abrogated protein disaggregation, again indicating competition for aggregate binding.

We next asked whether ClpL from other Gram-positive bacteria also exhibits high disaggregation activity. We selected *Lactobacillus gasseri* (*Lg*) ClpL, as this bacterium does not encode for the canonical disaggregase ClpB and *ΔclpL* cells exhibit a loss of heat resistance (Figure 1D) (Suokko *et al.*, 2008). *Lg* ClpL exhibited high disaggregation activity towards aggregated Luciferase and MDH that was similar to *Lm* ClpL (Figure 1E). This explains why *Lg ΔclpL* cells are heat-sensitive, as they lost the central disaggregase.

Together our findings establish ClpL as potent, autonomous disaggregase, whose disaggregation activity is comparable to ClpG. Our findings are different from former, initial analyses on ClpL from *Strepotoccus sp* reporting on either no (Tao & Biswas, 2013) or low disaggregation activity (Park *et al.*, 2015) towards single model substrates tested.

Specific features distinguish ClpL from the KJE/ClpB disaggregase

Lm ClpL exhibits superior disaggregation activity as compared to *Lm* KJE/ClpB. We speculated that ClpL applies a higher threading power, enabling it to process tight protein aggregates, which are largely resistant to KJE/ClpB activity. We made use of the fusion construct

Luciferase-YFP, which forms mixed aggregates at 46°C that consist of unfolded Luciferase and native YFP moieties (Figure 2A). Threading power can be assessed by monitoring YFP fluorescence during the disaggregation process. *Ec* KJE/ClpB and *Lm* KJE/ClpB did not unfold YFP during the disaggregation process, documenting limited unfolding power, consistent with former reports (Haslberger *et al.*, 2008; Katikaridis *et al.*, 2019). In contrast, we observed a rapid loss of YFP fluorescence in presence of ClpL that was even faster as compared to ClpG (Figure 2B). We conclude that stand-alone disaggregases ClpL and ClpG but not the canonical KJE/ClpB disaggregase exhibit robust threading activities that allow for unfolding of tightly folded domains.

ClpL strongly enhances survival of *Lm* cells at 55°C, a temperature that is far beyond the maximum growth temperature (45°C) of *Lm* cells. We speculated that these high temperatures inactivate KJE/ClpB activity by thermal unfolding of one of the chaperones involved. We therefore determined the thermal stabilities of ClpL and the central components DnaK and ClpB of the bi-chaperone disaggregase by monitoring protein unfolding during temperature increase via SYPRO®Orange binding and nanoDSF (Figure 2C/D). *Lm* ClpL and ClpB exhibited comparable melting temperatures of 60°C-63°C, while the thermal stability of *Lm* DnaK was much lower (T_M: 47°C-50°C) (Figure 2C/D). We infer that incubation at 55°C will cause unfolding of *Lm* DnaK, thereby abrogating KJE/ClpB disaggregation activity. The higher thermal stability of ClpL will provide disaggregation power to *Lm* cells at 55°C, explaining its strong protective effect on bacterial survival.

The N-terminal domain of ClpL mediates aggregate targeting

We explored the mechanistic basis of ClpL disaggregation activity. We first tested for roles of its AAA1/2 domains by mutating glutamate residues of the Walker B motifs (E197A, E520A), crucial for ATP hydrolysis, and aromatic pore loop residues (Y170A, Y504A), involved in substrate threading (Figure 3 – figure supplement 1A). ClpL wild-type (WT) exhibits high, concentration-independent ATPase activity (90.1 ± 26.1 ATP/min/monomer) (Figure 3 – figure supplement 1B). ATPase activities of pore loop mutants were similar to WT, while they were strongly reduced in Walker B mutants (Figure 3 – figure supplement 1C). A ClpL pore-1 loop mutant (Y170A) retained partial disaggregation activity, while blocking ATP hydrolysis in one AAA domain (E197A, E520A) or mutating the pore-2 site (Y504A) abrogated disaggregation (Figure 3 – figure supplement 1D). These findings are similar to phenotypes of corresponding ClpB and ClpG mutants and underline that two functional AAA domains and an intact pore-2 site are crucial for disaggregation activity.

We next turned our interest to the N-terminal domain (NTD) of ClpL, which is distinct from the NTDs of ClpG and ClpB (Figure 1 – figure supplement 1). NTDs are connected via flexible linkers to the AAA ring structure and typically mediate substrate or partner specificity (Kirstein *et al*, 2009). We deleted the NTD (ΔN: ΔA2-N61)) of ClpL and observed a total loss of disaggregation activity towards Luciferase and MDH aggregates (Figure 3A). ATPase activity of ΔN-ClpL was hardly affected (Figure 3B), excluding basic structural defects as reason for disaggregation activity loss. To explore the role of the NTD for disaggregation activity in an *in vivo* setting, we expressed ClpL and ΔN-ClpL in *E. coli ΔclpB* cells and monitored the recovery of aggregated Luciferase (Figure 3C). Expression of *clpL* but not *ΔN-clpL* allowed for regain of Luciferase activity (16.5 % (WT) vs 1.6 % (ΔN-ClpL) after 120 min at 30°C). ClpL disaggregation activity was lower than *Pa* ClpG activity but higher than *Ec* ClpB activity, which served as references. Expression of *clpL,* but not *ΔN-clpL,* also restored thermotolerance in *E. coli ΔclpB* and *dnaK103* mutant cells, lacking a functional DnaK chaperone (Figure 3D, Figure 1 – figure supplement 2A). Expression levels of disaggregases in *ΔclpB* and *dnaK103* were comparable (Figure 1 – figure supplement 2B/C). These data underline the robust, autonomous disaggregation activity of ClpL and document the essential role of its NTD.

This role of the NTD in aggregate targeting can explain the defect of ΔN-ClpL in protein disaggregation. To directly demonstrate this function, we fused the ClpL NTD to ΔN-ClpB-K476C (ΔN-ClpB*) generating L_N-ClpB* (Figure 3E). The K476C mutation is located in the ClpB MD, abrogating ClpB repression and allowing for high ATPase activity in the absence of DnaK. L_N-ClpB* exhibited high disaggregation activity, whereas ClpB* and ΔN-ClpB* relied on the presence of the cooperating DnaK (KJE) system (Fig 3F). Thus, fusion of ClpL NTD converts ClpB into a stand-alone disaggregase bypassing the need of DnaK for aggregate targeting.

Molecular principle of aggregate recognition by ClpL

To understand how the ClpL NTD selectively interacts with protein aggregates we predicted its structure with AlphaFold2 (Jumper *et al*, 2021; Mirdita *et al*, 2022) and validated this model by nuclear magnetic resonance spectroscopy (NMR). AlphaFold2 predicts a conformation of two α-helices (α1, α2) and a short anti-parallel β-sheet, while N- and C-terminal regions are disordered (Figure 4A). The β-sheet forms a small hydrophobic core with α2, which in turn is predicted to interact with α1, forming a second small core structure (Fig. 4A). The latter hydrophobic core is formed mostly by π-stacking interactions of four aromatic residues (F19, F23, Y36 and F48, Figure 4B) and the side chain methyl group of A34. The C-terminal hydrophobic core is formed by residues Y36, V38, L43, F48, Y51 and L57. Thus, Y36 and F48 would take part in the formation of both hydrophobic cores. The ^{15}N-HSQC NMR spectrum of the NTD shows several well-dispersed resonances, indicative of a folded domain (Figure 4 – figure supplement 1A). NMR secondary chemical shifts based on Cα and Cβ backbone resonance assignments confirm the formation of α2 and the β-sheet and thus validate partly the structure prediction (Figure 4B). However, although a certain helical propensity can be confirmed from secondary chemical shifts for α1, the formation seems rather transient compared to α2. While NOEs between relevant residues confirm the existence of the C-terminal hydrophobic core (Figure 4 – figure supplement 1B/C), long-range NOEs, expected to arise based on the predicted tertiary interactions between α1 and α2 are entirely missing and only intra-residue or sequential NOEs are visible (Figure 4 – figure supplement 1B, D). This indicates that the ClpL NTD forms one predicted folded core structure but that α1 forms only transiently and does not interact with α2. To further confirm this, we acquired ^{15}N spin relaxation data to measure residue-wise dynamics in the ps-ns time scale (Figure 4 – figure supplement 1E). Longitudinal (R_1) and transverse (R_2) relaxation rates and heteronuclear NOE data clearly show that the N-terminal region up to residue A34 is more flexible than the hydrophobic core formed by α2 and the β-sheet. The overall low heteronuclear NOE values, rarely above 0.6 also indicate that the secondary structure elements (α1 vs. α2/β-sheet) are mobile with respect to each other in the ps-ns time scale. These observations are consistent with pLDDTs that are generally <70 and partially <50 in AlphaFold2 predictions (Figure 4A). Thus, the NTD is highly mobile and formed by a hydrophobic core between secondary structure elements α2 (D46-T54) and the β-sheet formed by residues R35-V38 and Q41-T44. The α-helix 1 forms only transiently and is mobile, i.e. does not interact with α2, thereby making several aromatic residues available for substrate binding.

Sequence analysis of multiple ClpL NTDs revealed a strongly increased frequency of asparagine (N) and glutamine (Q) residues, while aliphatic residues were less abundant compared to their average occurrence in bacterial proteomes (Figure 4C). These sequence features can explain the lack of a stable compact NTD structure. We also noticed an increased frequency of phenylalanine residues. We found aromatic and N/Q residues are frequently located together in patches (A-E), which are all located outside the small α2/β-sheet core (Figure 4D). To explore the role of those patches and of the high aromatic and N/Q content for substrate binding and protein disaggregation activity, we replaced aromatic and N/Q residues

of individual patches with alanines (e.g. patch A: 3NFY5 to 3AAA5). Alternatively, we mutated all aromatic or all N/Q residues present in patches A-E to alanines (all Aro/Ala, all NQ/Ala). All ClpL NTD mutants showed high ATPase activities, excluding severe assembly defects or direct effects on ATP hydrolysis (Figure 4 – figure supplement 2A). We only observed a 3.6-fold reduced ATPase activity for the "all Aro/Ala" construct at low protein concentrations (0.125 μM). At the concentration used in the disaggregation assay (1 μM), no differences to ClpL WT were determined (Figure 4 – figure supplement 2A).

All NTD mutants were tested for disaggregation activity towards aggregated Luciferase and MDH (Figure 4E). Replacement of aromatic residues (all Aro/Ala) abrogated disaggregation while mutating all N/Q residues had no effect ((Figure 4 – figure supplement 2A). Patch A and C mutants exhibited reduced (Luciferase) or lost (MDH) disaggregation activities. The loss of disaggregation activity of selected NTD mutants (ΔN, all Aro/Ala) could be linked to a deficiency in binding aggregated Luciferase (Figure 4F), indicating a crucial role of aromatic residues in aggregate recognition. In an additional set of experiments we combined alternative patch A-C mutants, in which only the aromatic residues were mutated and generated single point mutations of aromatic residues being part of the α2/β-sheet core (Y36A, F48A, Y51A) ((Figure 4 – figure supplement 2B). All patch combinations showed aggravated disaggregation activities as compared to single patch mutants. Furthermore, disaggregation activity of ClpL-Y51A but not Y36A and F48 was severely affected (Figure 4 – figure supplement 2B/C). None of these mutants were affected in ATP hydrolysis ((Figure 4 – figure supplement 2D).

We finally recapitulated the effect of key NTD mutations in the L_N-ClpB* fusion construct. We confirmed the crucial function of aromatic residues in patches A – C, yet the Y51A did not exhibit the same severe phenotype as observed for ClpL, suggesting a context-specific role ((Figure 4 – figure supplement 2E/F). Defects in protein disaggregation were again linked to defects in aggregate binding, whereas ATPase activities of all mutants tested were similar to the L_N-ClpB* reference (Figure 4 – figure supplement 2G/H). Together these findings indicate an important role of aromatic residues in the flexible N-terminal region of ClpL for disaggregation activity. Our data suggest that the total number of aromatic residues but also their particular identity represent crucial parameters for substrate binding.

We next determined how many NTDs must be present in a ClpL ring to achieve high disaggregation activity. We speculated that ClpL might utilize multiple NTDs to simultaneously contact various binding sites present in close vicinity on an aggregate surface. Such recognition principle would specifically target ClpL to an aggregate while preventing ClpL action on soluble, non-native polypeptides (e.g. nascent polypeptide chains). We performed mixing experiments using L_N-ClpB* and ΔN-ClpB* as model system, since ClpB hexamers dynamically exchange subunits ensuring stochastic formation of mixed hexamers (Figure 5A/B) (Haslberger *et al.*, 2008; Werbeck *et al*, 2008). We confirmed mixing of WT and mutant subunits by showing that the presence of ATPase deficient ΔN-ClpB*-E218A/ E618A, harboring mutated Walker B motifs in both AAA domains, strongly poisoned disaggregation activity of L_N-ClpB* (Figure 5 – figure supplement 1A). Similarly, presence of an excess of ΔN-ClpB* inhibited L_N-ClpB* (Figure 5 – figure supplement 1B). We determined the disaggregation activities of mixed L_N-ClpB*/ΔN-ClpB* hexamers formed at diverse mixing ratios. The determined activities were compared to those derived from a theoretical model assuming that a mixed hexamer only displays activity if it contains a certain number of L_N-ClpB* subunits (Figure 5B, Figure 5 – figure supplement 1C-E). This comparison revealed that approx. four to five ClpL NTDs domains must be present in a hexamer to confer high disaggregation activity. In a reciprocal approach we tested whether an isolated NTD can inhibit L_N-ClpB* or ClpL disaggregation activity by competing for aggregate binding (Figure 5C/D). Addition of up to a 50-fold excess of ClpL NTD did not reduce disaggregation activities. This suggests a vast increase in binding affinities of AAA+ rings harboring multiple ClpL NTDs to protein aggregates and explains efficient outcompetition of isolated NTD by hexamers.

Functional relevance of diverse ClpL assembly states

Streptococcus pneumoniae ClpL has been recently described as tetradecameric species, which forms by interaction of two heptameric rings via head-to-head interactions of coiled-coil MDs (Kim *et al*, 2020) (Figure 6A). This assembly state is suggested to represent the active species of ClpL, however, it will render the NTDs largely inaccessible for aggregate binding. We therefore monitored *Lm* ClpL oligomerization by SEC and negative staining EM. ClpL eluted prior to ClpB in SEC runs, indicating the formation of assemblies larger than hexamers (Figure 6 – figure supplement 1A). EM analysis revealed that ATPγS-bound ClpL adopts diverse assembly states including single hexameric and heptameric rings, dimers of rings and a tetrahedral structure formed by four ClpL rings (Figure 6B). A tetrahedral structure is also formed by the bacterial AAA+ member ClpC upon binding of activating compounds (Maurer *et al*, 2019; Morreale *et al*, 2022; Taylor *et al*, 2022). The structural plasticity of ClpL is therefore much larger than originally anticipated. Dimers and tetramers of ClpL rings form by MD-MD interactions as ClpL-ΔM (ΔD330-Q376) or MD mutants (E352A, F354A) (Figure 6 – figure supplement 1B) only form single hexameric and heptameric rings and accordingly eluted much later in SEC runs as compared to ClpL-WT (Figure 6C, Figure 6 – figure supplement 1A/C). Notably, ΔN-ClpL only forms dimers of rings, suggesting that NTD presence destabilizes this assembly state (Figure 6C, Figure 6 – figure supplement 1C). An increased rigidity of ΔN-ClpL is also supported by a higher T_M-value as compared to ClpL-WT and ClpL-ΔM (Figure 6 – figure supplement 1D). EM analysis of selected NTD point mutants revealed minor changes in the fractions of individual structural states as compared to ClpL-WT but did not resemble ΔN-ClpL (Figure 6 – figure supplement 1E), suggesting that the mere presence of the NTD destabilizes a dimer of rings through steric clashes.

Disaggregation activities of ClpL MD mutants were either similar to WT (E352A) or partially reduced (F354A) (Figure 6D/E). ClpL-F354A also exhibited a reduced ATPase activity, particularly at low protein concentrations (Figure 6 – figure supplement 1F). *Lg* ClpL, which is highly active in disaggregation assays (Figure 1E), forms hexamers as most abundant structural state (69 %) (Figure 6C). We infer that single ClpL rings represent functional disaggregases, questioning a specific role of ring dimers in protein disaggregation. Our data also imply that ClpL activity is not restricted to a heptameric state as suggested before (Kim *et al.*, 2020).

To study the role of dimers of rings in protein disaggregation, we generated the MD mutant ClpL-T355C, which allowed for disulfide bond formation between interacting MDs under oxidizing conditions (Figure 6F). This enabled us to probe for the consequences of stabilizing ClpL ring dimers through covalent linkages on disaggregation activity. T355C purified under reducing conditions (+ DTT) exhibited slightly reduced disaggregation and ATPase activities as compared to ClpL-WT (Figure 6 – figure supplement 2A/B). Disulfide bond formation and breakage upon removal and re-addition of DTT was verified by SDS-PAGE (Figure 6F) and formation of ring dimers was confirmed by EM (Figure 6 – figure supplement 2C). Luciferase disaggregation activities of ClpL-WT and ClpL-T355C were assessed in absence and presence of DTT. The assay was in general sensitive to the presence of DTT, leading to an overall increase of Luciferase reactivation by 2.7-fold for ClpL-WT, likely due to the fact that Firely Luciferase itself possesses multiple cysteines. Importantly, we observed a much stronger activity gain of ClpL-T355C under reducing conditions as compared to ClpL-WT (2.8 ± 0.4-fold vs 6.6 ± 1.3-fold, respectively) (Figure 6G). Re-addition of DTT strongly increased ClpL-T355C disaggregation activity, which was now similar to ClpL-WT. In an alternative approach, we monitored the unfolding activities of oxidized and reduced ClpL-WT and ClpL-T355C towards mixed Luciferase-YFP aggregates (Figure 6 – figure supplement 2D). Here, we followed the loss of YFP fluorescence as readout for disaggregation activity as we assumed that the unfolding reaction is more independent on DTT. Indeed, the activity of oxidized WT remained largely unaffected (1.4 ± 0.5-fold increase in activity with DTT). In striking contrast,

ClpC-T355C showed massive loss in disaggregation activity in absence of DTT but became fully active upon DTT re-addition (18.2 ± 7.4-fold increase in activity with DTT). We infer that stabilizing ClpL ring dimers through covalent linkage strongly reduces disaggregation activity.

Discussion

In the presented work we describe the bacterial AAA+ member ClpL as potent and partner-independent disaggregase that confers enhanced heat resistance to *Lm*. The presence of ClpL on transmissible plasmids in *Lm* poses a severe risk on food safety as it substantially increases the survival rate of the pathogen in adverse environments like food processing plants. It also explains the high prevalence of the *clpL* gene in *Listeria* species isolated from ready-to-eat foods and dairy products (Parra-Flores *et al*, 2021; Ramadan *et al*, 2023).

ClpL shares various features with the recently described stand-alone ClpG disaggregase, which is linked to superior thermotolerance in selected Gram-negative bacteria, qualifying ClpL as ClpG counterpart in Gram-positive species. Our analysis of ClpL and previous findings on ClpG allow to define five features shared by both novel disaggregases.

First, ClpL and ClpG exhibit a higher threading power as compared to the canonical ClpB disaggregase. ClpB unfolding power is repressed by intersubunit interactions of its long coiled-coil MDs (Deville *et al*, 2017). The shortened lengths of ClpL and ClpG MDs explain why this inhibitory mechanism is not operative in the novel disaggregases. Increasing ClpB threading activity by MD mutations is linked to severe cellular toxicity, rationalizing ClpB limitations (Lipinska *et al*, 2013; Oguchi *et al*, 2012). The increased unfolding power of ClpL/ClpG is linked to higher disaggregation activities as shown for various aggregated model proteins in this work. We suggest that an enhanced threading activity will become particularly important upon extreme heat shock, which causes more complete unfolding of proteins. This will increase the number of interactions between proteins trapped inside an aggregate, thus demanding for an enhanced threading force for efficient disaggregation.

Second, ClpL and ClpG are more thermostable as compared to the DnaK/ClpB bi-chaperone disaggregase present in corresponding bacterial species. The T_M value (46-50°C) of *Lm* DnaK might represent a limiting factor for *Lm* survival at temperatures above 46°C as loss of DnaK by thermal unfolding will abrogate DnaK/ClpB disaggregation activity. This will leave *Lm* cells unprotected against severe heat stress unless they harbour plasmid-encoded ClpL, which resists unfolding up to 60°C. Notably, unfolding of DnaK at high temperatures will abrogate the observed competition between DnaK and ClpL for aggregate binding, enabling for undisturbed activity of the more powerful disaggregase. Similarly, *Ec* ClpG is more heat stable than *Ec* DnaK (T_M values of 69°C and 59°C, respectively) (Kamal *et al*, 2021a; Palleros *et al*, 1992) and dramatically increases cell survival at 65°C. We infer that increased heat resistance provided by novel disaggregases is reflected in their enhanced thermostability.

Third, distinct NTDs enable novel disaggregases to directly bind to protein aggregates, making them independent of partner proteins. ClpL and ClpG NTDs do neither exhibit sequence nor structural homology, however, both use hydrophobic or aromatic residues for aggregate recognition (Katikaridis *et al*, 2023). The ClpL NTD only adopts a partially stable core structure with regions featuring aromatic residues being mobile and accessible, suggesting that it represents a sticky tentacle that interacts via aromatic residues with hydrophobic patches present on an aggregate surface. This binding mode is reminiscent to small heat shock proteins, which interact via disordered NTDs enriched in aromatic residues with substrates (Kriehuber *et al*, 2010; Shrivastava *et al*, 2022). Both, ClpL and ClpG, require simultaneous binding of multiple NTDs to protein aggregates for high disaggregation activities (Katikaridis *et al.*, 2023), indicating that they increase binding affinity through avidity effects. This principle provides substrate specificity while sparing non-aggregated protein species from potentially harmful threading and unfolding activities.

Forth, novel disaggregases do not cooperate with the peptidase ClpP as they lack the specific IGL/F signature motif. This feature is shared with the canonical ClpB disaggregase (Weibezahn *et al*, 2004) and ensures that protein disaggregation is primarily linked to protein refolding. This also underlines that it is the loss of essential proteins upon heat-induced aggregation that represents the major limiting factor for bacterial viability.
Fifth, novel disaggregases are typically encoded on transmissible plasmids or mobile genomic islands. ClpL present in other Gram-positive bacteria is either encoded on plasmids (Huang *et al*, 1993) or is part of the core genome and can be flanked by inverted repeat sequences and truncated transposase genes, suggesting acquisition via horizontal gene transfer (Suokko *et al.*, 2005). Notably, prolonged cultivation at high temperatures can lead to mobilization of chromosomal-encoded *clpL* (Suokko *et al.*, 2005). We infer that novel disaggregases can be acquired by horizontal gene transfer, leading to spreading of bacterial resistance towards severe heat stress in Gram-positive and Gram-negative bacteria.

Lm ClpL displays remarkable structural plasticity by forming hexameric and heptameric rings that can interact via MDs forming higher assembly states. This confirms and expands a former report on *S. pneumoniae* ClpL (Kim *et al.*, 2020). ClpL MD mutants, which only form single hexameric rings remain functional disaggregases and, similarly, the disaggregase *Lg* ClpL mostly forms single hexamers. This suggests that single rings of ClpL represent the active species. The aggregate-targeting NTDs will be obstructed in dimers and tetramers of rings precluding ClpL binding to an aggregated protein. Accordingly, stabilizing ring dimers via covalent linkage leads to a loss of ClpL disaggregation activity. The finding that ClpL-ΔN exclusively forms dimers of rings implies that NTDs destabilize such structural state and increase ring dynamics, ensuring their accessibility.
The formation of ring dimers is also observed for other AAA+ family members and their functional roles are currently actively discussed. p97 double rings form by ATPase ring interactions and are suggested to represent a potentiated state (Gao *et al*, 2022). Dodecamers of the bacterial AAA+ protease Lon regulate substrate selectivity and mostly exhibit reduced proteolytic activity (Vieux *et al*, 2013). The role of ring dimers of the human mitochondrial disaggregase Skd3 in protein disaggregation is controversial and both, higher and lower disaggregation activity has been associated with this state (Cupo *et al*, 2022; Gupta *et al*, 2023; Lee *et al*, 2023; Spaulding *et al*, 2022; Wu *et al*, 2023). The mechanistic role of ClpL ring assemblies remains to be explored. We speculate that they might represent storage states, reducing ClpL activity by shielding NTDs. Studying the dynamics and regulations of ClpL ring interactions will become crucial for understanding ClpL activity control.

Materials and methods

Strains and plasmids

All strains and plasmids used in this study are summarized in Table S1. *Escherichia coli* cells were grown in LB medium at 30°C containing appropriate antibiotics (kanamycin (50 µg ml^{-1}), ampicillin (100 µg ml^{-1}) and spectinomycin (50 µg ml^{-1}) , shaking at 120 rpm. Deletion mutants and L_N-ClpB* hybrids were generated by PCR/restriction cloning, point mutants were constructed via PCR-based mutagenesis. ClpL NTD mutants A-E were generated utilizing synthetic DNA as template (Invitrogen™) and restriction cloning. All constructs were verified by sequencing.

Protein purification

E. coli ClpB (WT and derivatives) was purified after overproduction from *E. coli* Δ*clpB::kan* cells using pDS56-derived expression vectors (Oguchi *et al.*, 2012). *P. aeruginosa* $ClpG_{GI}$, *Lm*

ClpL (wt, NTD-mutants and isolated NTD), *L. gasseri* ClpL and components of the *L. m* BKJE-system were purified after overproduction in *E. coli* BL21 cells using pET24a-derived expression vectors. ^{15}N single-labeled and ^{15}N-^{13}C double-labeled ClpL NTDs for NMR were produced in *E. coli* BL21 cells in M9 medium with 1g/l $^{15}NH_4Cl$ and 2 g/l ^{13}C-glucose. *Lm* ClpL MD-mutants and L_N-ClpB* fusion constructs were overexpressed in *E. coli* BL21 cells from pCA528 and pC6AmpΔBsaI expression vectors, fusing an Ulp1 cleavable 6x His + SUMO-tag to the N-termini, protecting the ClpL N-termini from cleavage upon cell lysis and allowing for selective purification of ClpL variants with intact NTDs.
All proteins were purified using Ni-IDA (Macherey-Nagel) following the instructions provided by the manufacturer. In short, cell pellets were resuspended in buffer A1 (50 mM NaH_2PO_4, 300 mM NaCl, 5 mM β-mercaptoethanol, pH 8.0) supplemented with protease inhibitors (8 µg/mL Pepstatin A, 10 µg/mL Aprotinin, 5µg/mL Leupeptin,) and DnaseI (5 µg/mL). For ClpL purifications a higher salt concentration was used in buffer A1* (50 mM NaH_2PO_4 pH 8.0, 1 mM NaCl, 5 mM β-mercaptoethanol), to reduce co-purification of partially cleaved monomers in assembled oligomers. After cell lysis using a French press the cell debris was removed by centrifugation at 17000 g for 1 h at 4 °C and the cleared lysate was incubated with Protino IDA resin (Macherey-Nagel) for 20 min at 4° C. Afterwards the resin was transferred into a plastic column and washed with at least 5 CV buffer A1, or in the case of ClpL, washed with at least 5 CV buffer A1* and then 5 CV buffer A1. His-tagged proteins were eluted by addition of buffer A1 supplemented with 250 mM Imidazole. For *Lm* DnaJ purification cell pellets were lysed in Lysis buffer J1 (50 mM Tris pH 7.9, 500 mM NaCl, 0,6 % Brij58, 5 mM MgCl2 1x DNAseI, cOmplete™ Mini EDTA-free protease inhibitor tablets (Roche)). The resin was first washed with at least 10 CV of Wash buffer J2 (50 mM Tris pH 7.9, 1.5 M NaCl, 0,1 % Brij58, 2 M Urea) and then with 20 CV of Wash buffer J3 (50 mM Tris pH 7.9, 500 mM NaCl, 2 mM β-Mercaptoethanol, 2 M Urea) to remove detergent. DnaJ was eluted with Elution buffer J4 (50 mM Tris pH 7.9, 500 mM NaCl, 2 mM β-Mercaptoethanol, 2 M Urea) and Imidiazole was removed via overnight dialysis in Storage buffer J5 (40 mM HEPES pH 7.6, 2 mM β-Mercaptoethanol, 300 mM KCl, 10% glycerol (v/v)) at 4 °C.
Except for DnaJ and the ClpL all NQ/Ala mutant all proteins were further purified via size exclusion chromatography (SEC). Prior to that SUMO-tagged proteins were incubated with Ulp1 for 1 h at room temperature to cleave off the His_6-SUMO tag. SEC runs were done with HiLoad® 16/600 Superdex® 200 pg (Cytiva) in buffer B1 (50 mM Tris pH 7.5, 50 mM KCl, 10 mM $MgCl_2$, 5% (v/v) glycerol, 2 mM DTT) for *E. coli* ClpB or buffer B2 (50 mM Tris pH 7.5, 50 mM KCl, 20 mM $MgCl_2$, 5% (v/v) glycerol, 2 mM DTT) for all others. In case of isolated ClpL NTD a HiLoad® 16/600 Superdex® 30 pg (GE Healthcare) was used in the SEC step. Proteins were concentrated with either Aquacide II (Merck) or Amicon® Ultra Centrifugal Filters. Isolated ClpL NTD was dialysed in NMR buffer (50 mM NaH_2PO_4 pH 6.5, 50 mM KCl, 2 mM DTT) overnight at 4 °C.
Purifications of *E. coli* DnaK, DnaJ, GrpE and Firefly Luciferase were performed as described previously (Haslberger *et al.*, 2008; Oguchi *et al.*, 2012; Seyffer *et al*, 2012). Pyruvate kinase of rabbit muscle and Malate Dehydrogenase of pig heart muscle were purchased from Sigma. Protein concentrations were determined with via Bradford assay (Bio-Rad Protein Assay Dye Reagent).

Biochemical assays

ATPase Assay

The ATPase activities of 0.125 µM or 1 µM ClpL, ClpL mutants and L_N-ClpB* were determined in a reaction volume of 100 µl in assay buffer (50 mM Tris pH 7.5, 50 mM KCl, 20 mM $MgCl_2$, 2 mM DTT) with 0.5 mM NADH (Sigma), 1 mM PEP (Sigma) and 1/100 (v/v) Pyruvate Kinase/Lactic Dehydrogenase mix (Sigma). 100 µl of 4 mM ATP in assay buffer (50 mM Tris pH 7.5, 50 mM KCl, 20 mM $MgCl_2$, 2 mM DTT) were added to each reaction in a 96-

well plate (TPP) format to start the reaction. The decrease of NADH absorbance at 340 nm was determined in a CLARIOstar® Plus Platereader (BMG Labtech) at 30 °C. ATPase activities were calculated assuming a 1:1 stoichiometry of NAD^+ oxidation and the production of ADP.

In vitro Disaggregation Assays

All disaggregation assays were performed in 50 mM Tris pH 7.5, 50 mM KCl, 20 mM $MgCl_2$, 2 mM DTT. Aggregates of 200 nM Luciferase were generated through incubation at 46°C for 15 min in assay buffer. Aggregates of 2 µM MDH were generated through incubation at 47°C for 30 min. Aggregates of 1 µM GFP were generated through incubation at 80°C for 10 min. Aggregates of 2 µM α-Glucosidase were generated through incubation at 47°C for 30 min. Equal volumes of protein aggregate suspensions were mixed with chaperones and an ATP regeneration system (15 mM PEP, 20 ng/µL Pyruvate Kinase). Reactions were started by addition of 2 mM ATP. If not stated otherwise final chaperone concentrations were: 1 µM ClpL, ClpG, ClpB, L_N-ClpB*, *Ec* KJE*:* 1 µM *Ec* DnaK, 0.2 µM *Ec* DnaJ, 0.1 µM *Ec* GrpE, *Lm* KJE: 1 µM *Lm* DnaK 0.5 µM *Lm* DnaJ, 0.25 µM *Lm* GrpE, 2x Lm KJE: 2 µM *Lm* DnaK 1 µM *Lm* DnaJ, 0.5 µM *Lm* GrpE). Reactions were kept at 30°C for the duration of the assay.

To determine Luciferase activities 2 µl were taken from each disaggregation reaction in regular time intervals and added to 100 µl Measurement Buffer (25 mM Glycylglycine pH = 7.4, 12.5 mM MgSO4, 5 mM ATP) inside a 5 ml reaction tube (Greiner). Luminescence was measured for 2 s in a Lumat LB 9507 (Berthold Technologies) after injection of 100 µl 250 nM Luciferin (Gold Biotechnology). Luciferase Refolding served as a measure for disaggregation activity, native Luciferase was used as a reference for the efficiency of recovery. Refolding rates (% Luciferase refolded/min) were calculated from the linear increase in Luciferase activities.

MDH refolding was measured in additional presence of 1 µM GroEL/ES to facilitate refolding of disaggregated MDH. 10 µl were taken from each disaggregation reaction in regular time intervals and mixed with 690 µL Measurement Buffer (150 mM Potassium phosphate pH 7.6, 0.5 mM Oxaloacetate, 0.28 mM NADH, 2 mM DTT) inside a 1 ml Polystyrene Cuvette (Sarstedt). MDH activity was quantified by measuring absorption at 340 nm every 10 s for 30 s on a Biochrom Novaspec Plus photometer. The activity of native MDH served as a reference to determine disaggregation efficiency. Refolding rates (% refolded MDH/min) were calculated from the linear increase in MDH activity.

Refolding of aggregated GFP was determined by monitoring regain of GFP fluorescence upon excitation at 400 nm was continuously recorded at 510 nm on a LS50B spectrofluorometer (PerkinElmer).

Disaggregation of α-Glucosidase was followed by continuously recording aggregate turbidity using 600 nm as excitation and emission wavelengths on a LS50B spectrofluorometer (PerkinElmer).

Luciferase-YFP-unfolding Assay

200 nM Luciferase-YFP (Luc-YFP) was subjected to heat-treatment at 46 °C for 15 min. 150 µl aggregate suspension was combined with the respective disaggregases. Reactions were started and sustained by addition of 2 mM ATP and an ATP-regeneration system (15 mM PEP, 20 ng/µL Pyruvate Kinase) in a final reaction volume of 300 µL. Chaperone concentrations were 1 µM ClpL, ClpG, ClpB, *Ec*/*Lm* DnaK, 0.2 µM *Ec* DnaJ, 0.5 µM *Lm* DnaJ, 0.1 µM *Ec* GrpE, 0.25 µM *Lm* GrpE). Reactions were kept in 1 mL UV quartz cuvettes at 30 °C for the duration of the assay. YFP fluorescence upon excitation at 505 nm was continuously recorded at 525 nm on a LS50B spectrofluorometer (PerkinElmer). Alternatively, fluorescence was tracked using a CLARIOstar® Plus Platereader (BMG Labtech). Here, the samples were scaled down to a total volume of 20 µl and loaded onto Black Polysterene Non-Binding 384 Assay Plates (Corning, flat bottom). The platereader assay was performed at room temperature, due

to positional bias of the heating function. The initial signal was set to 100 % for each sample. Unfolding rates were calculated from the linear phase of YFP fluorescence decrease.

Protein aggregate binding assay

To examine the interaction between ClpL or L_N-ClpB* with protein aggregates, 4 µM MDH was heat-denatured at 47 °C for 30 min in assay buffer (50 mM Tris pH 7.5, 50 mM KCl, 20 mM $MgCl_2$, 2 mM DTT). MDH aggregates were mixed with 1.5 µM ClpL and 2 mM of ATPγS in 100 µl assay buffer and incubated at 25 °C for 10 min. Soluble and insoluble fractions were separated by centrifugation at 13,000 rpm for 25 min at 4 °C. The pellet fraction was washed once with 150 µl assay buffer and centrifuged again at 13,000 rpm for 10 min at 4 °C. Binding assays were performed in Low binding micro tubes (Sarstedt). Supernatant and pellet fractions were mixed with protein sample buffer and analyzed by Coomassie staining after SDS-PAGE. As a control, ClpL or L_N-ClpB* without aggregated proteins was subjected to the same protocol. Band intensities were analyzed using ImageJ.

Determination of T_M values by SYPRO®Orange binding and nanoDSF

Thermal stability of protein samples was monitored in a thermal shift assay with SYPRO®Orange (ThermoFisher Scientific) on a LightCycler® 480 II (Roche). All proteins were dialysed and stored in HEPES storage buffer (50 mM HEPES pH 7.5, 50 mM KCl, 20 mM $MgCl_2$, 5 % Glycerole) to reduce thermally induced pH changes.

Chaperones were incubated at concentration of 1 µM with 2 mM of the respective Nucleotide (ATPγS/ATP/ADP) in HEPES low salt buffer (50 mM HEPES pH 7.5, 50 mM KCl, 20 mM $MgCl_2$) in a total volume of 50 µl for 1 h (ATPγS) or 5 min (ATP/ADP) to allow for the formation of a stable distribution of oligomeric species. Subsequently, SYPRO®Orange (from 5000x commercial stock) was added to a final concentration of 80x and the samples were loaded onto a LightCycler® 480 Multiwell Plate 384. SYPRO®Orange Fluorescence was recorded over a temperature range from 20 °C to 95 °C. NanoDSF (differential scanning fluorimetry) measurements were performed on a Prometheus Panta from NanoTemper Technologies GmbH. Chaperone and nucleotide concentrations were the same as for the SYPRO® experiments, only for DnaK a chaperone concentration of 10 µM was used, due to insufficient signal at lower concentrations. T_M-values were derived from inflection points based on sigmoidal curve fits (https://gestwickilab.shinyapps.io/dsfworld/) for SYPRO® Orange data, while T_M-values for NanoDSF were directly calculated with the NanoTemper Analysis Software.

Disulfide crosslinking

For the purification of disulfide-bond stabilized ClpL T355C-tetradecamers (and ClpL WT controls), 5 mM β-Mercapoethanol (β-Me) was present in all steps up to the SEC, to prevent unspecific disulfide-bond formation. 2 mM ATP was added during the elution step from the Ni-IDA resin and into the SEC running buffer (50 mM Tris pH 7.5, 50 mM KCl, 20 mM $MgCl_2$, 10 % Glycerole) to allow for efficient and correct ring assembly. No reducing agent was added during any of the later steps, while remaining β-Me was removed during the SEC. The samples were processed immediately and freeze/thaw steps of the reducing agent-free samples were avoided. Addition of oxidizing compounds (e.g. Cu^{2+}-Phenanthrolin) only slightly enhanced disulfide bond formation but also led to damage of ClpL-WT and was therefore avoided. The efficiency of the crosslinking was determined via SDS-PAGE, by comparing the ratio between ClpL dimers and monomers, whereas the overall quality of the assembly was assessed via negative stain EM. ClpL T355C samples that showed a crosslinking efficiency of approx. 75 % or higher were analyzed in two activity assays, with and without prior incubation of the chaperone with 10 mM DTT for 30 min at room temperature. (I) First, in a variant of the Luciferase Refolding assay, in which the assay buffer included 5 µM β-Me instead of 2 mM DTT, increasing Luciferase refolding without breaking disulfide-bonds. (II) Second, in the

Luciferase-YFP-unfolding assay, which was conducted without any further addition of reducing agent, except for the DTT added to indicated samples.

Analytic size exclusion chromatography

Oligomerization of ClpL WT and mutants was investigated by size exclusion chromatography (SEC) using a Superose® 6 10/300 GL column (GE Healthcare) at 4°C in assay buffer supplemented with 2 mM ATP. 6 µM protein was incubated for 5 min at room temperature with ATPγS before injection. Elution fractions were analysed via SDS-PAGE followed by staining with SYPRO™ Ruby (Invitrogen™) according to manufacturer protocols. Bio-Rad Gel Filtration Standard served as a reference.

Bioinformatic analysis

Multiple sequence alignments were performed using Clustal Omega (https://www.ebi.ac.uk/Tools/msa/clustalo/) and were displayed using Jalview. An incomplete 3D model of *Lm* ClpL was generated by SWISS-MODELL (https://swissmodel.expasy.org) using pdb-file 6LT4 as template (*S. pneumoniae* ClpL).

Heat Resistance Assay

E. coli Δ*clpB* or *dnaK103* cells harboring pUHE21/pDS56 derivates allowing for IPTG controlled expression of *E. c. clpB, dnaK,* P.a. *clpG*, *Lm clpL* and Δ*N-clpL* were grown in LB media at 30 °C to early logarithmic phase (OD_{600}: 0.15 – 0.2). Expression of the respective proteins was induced by addition of IPTG (*clpB*: 10 µM, *dnaK*: 100 µM *clpG*: 100 µM, *clpL*: 100 – 500 µM). Protein production was documented 2 h after IPTG addition by SDS-PAGE and western blot analysis using ClpL-specific antibodies. Subsequently one ml aliquots were shifted to 49°C for 120 min. At indicated time points bacterial survival was determined by preparing serial dilutions, spotting them on LB plates followed by incubation for 24 h at 30 °C.

***In vivo* Luciferase Disaggregation Assay**

For *in vivo* luciferase disaggregation *E. coli ΔclpB* cells harboring *placIq-luciferase* (for constitutive expression of Luciferase) and either *pUHE21-clpB, pUHE21-clpG, pDS56-clpL or pUHE21-*Δ*N-clpL* were grown in LB medium supplemented with ampicillin (100 µg/ml) and spectinomycin (50 µg/ml) at 30°C to early-logarithmic growth phase. *Chaperone* expression was induced by addition of IPTG (10 µM ClpB, 100 µM ClpG, 100/500 µM for ClpL WT or ΔN-ClpL) for 2 h. Production of chaperones to similar levels was verified by SDS-PAGE and subsequent Coomassie staining. Luciferase activities were determined in a Lumat LB 9507 and set to 100 %. For that, 100 µl of cells were transferred into 5 ml reaction tubes (Greiner), 100 µl of 250 nM Luciferin were injected and luminescence was measured for 10 s. Next, 900 µl aliquots of cells were shifted to 46°C for 15 min. Immediately afterwards, tetracycline (70 µg/ml) was added to stop protein synthesis and cells were moved back to 30°C. Luciferase activities were determined in regular intervals for 2 h.

Western Blotting

Total extracts of cells were prepared and separated by SDS-PAGE, which was subsequently electrotransferred onto a PVDF membrane. The membrane was incubated in the blocking solution (3% bovine serum albumin (w/v) in TBS) for 1 h at RT. Protein levels were determined by incubating the membrane with ClpL-specific antibodies (1:10,000 in TBS-T + 3% (w/v) bovine serum albumin) and an anti-rabbit alkaline phosphatase conjugate (Vector Laboratories) as the secondary antibody (1:20,000). Blots were developed using ECF Substrate (GE Healthcare) as the reagent and imaged via Image-Reader LAS-4000 (Fujifilm). Band intensities were quantified with ImageJ.

Electron microscopy and image processing

Negative staining, data collection and processing were performed as described previously (Gasse *et al*, 2015). 1 µM ClpL samples were preincubated in presence of 2 mM ATPγS for 5 min at room temperature and diluted immediately before application to a final concentration of 250 nM (except ClpL E352A and F354A (200 nM) and *Lg* ClpL (400 nM)). 5 µl sample was applied to a glow-discharged grid covered with an approximately 6–8-nm-thick layer of continuous carbon. After incubation for 5 s, the sample was blotted on a Whatman filter paper 50 (1450-070) and washed with three drops of water. Samples on grids were stained with 3 % aqueous uranyl acetate. Images were acquired on a Thermo Fisher Talos L120C electron microscope equipped with a Ceta 16M camera, operated at 120 kV. The micrographs were acquired at 57,000 × magnification (resulting in 2.26 Å per pixel) using EPU software. For 2D classification 20k particles (for *Lg* ClpL 25k) were selected using the boxer in EMAN2 (Tang *et al*, 1998). Image processing was carried out using the IMAGIC-4D package (van Heel *et al*, 1996). Particles were band-pass filtered, normalized in their gray value distribution and mass centered. Two-dimensional alignment, classification and iterative refinement of class averages were performed as previously described (Liu & Wang, 2011). For quantification only 4 unambiguously identifiable types of classes were considered: ClpL hexameric-ring top views, ClpL heptameric-ring top views, ClpL double-ring side views and ClpL tetramers-of-rings. Classes of partial assemblies, contaminants and picking related artifacts were not included in the quantification. Effective sample sizes were: ClpL WT = 5233, ClpL ΔN = 18314, ClpL ΔM = 1900, ClpL E352A = 14215, ClpL F354A = 7074, ClpL AB = 3588, ClpL C = 7404, ClpL all Aro/Ala = 9655, *Lg* ClpL = 11765.

Nuclear magnetic resonance spectroscopy

All NMR experiments were recorded at 298 K using Bruker Avance III NMR spectrometers operating at magnetic field strengths, corresponding to ^{1}H Larmor frequencies of 600, 700 and 800 MHz. The 600 and 800 MHz spectrometers were equipped with a cryogenic triple-resonance probe (the 700 MHz spectrometer was equipped with a room-temperature triple resonance probe). Protein concentrations were in the range between 200 and 620 µM. Backbone and side chain assignments were obtained using standard ^{1}H,^{13}C,^{15}N scalar correlation experiments (Sattler *et al*, 1999) employing apodization weighted sampling (Simon & Kostler, 2019). The data were processed with NMRpipe (Delaglio *et al*, 1995) and analysed with Cara (http://cara.nmr.ch) and Sparky (Lee *et al*, 2015). Secondary structure determination was based on secondary chemical shifts (Cβ and Cα) was performed according to the study by Wishart and Sykes (Wishart & Sykes, 1994). NOEs for validation of AlphaFold2 structure predictions were obtained from ^{1}H,^{1}H-2D NOESY (in D_2O), ^{15}N- and ^{13}C-edited 3D NOESY-HSQC, and ^{13}C-edited 3D HMQC-NOESY (in D_2O) experiments. NOE assignments were performed manually using Cara.

^{15}N spin relaxation parameters R_1, R_2, and heteronuclear NOEs were recorded on the 600 MHz Avance III spectrometer at 298 K. For R_1 experiments, relaxation delays of 50, 100, 150, 200, 300, 400, 500, 700 and 1000 were used, where the 50, 500 and 700 ms delay were acquired in duplicates to estimate peak volume uncertainties. For R_2 experiments, relaxation delays of 16, 32, 64, 96, 112, 128, 160, 192, 224 and 256 ms were used, where the 16 and 64 ms delays were acquired in duplicates to estimate peak volume uncertainties. For ^{15}N spin relaxation data analysis (peak volume, exponential fitting and calculation of relaxation rates) the program PINT was used (Ahlner *et al*, 2013; Niklasson *et al*, 2017).

Acknowledgments

V.B. and P.K. was supported by the Heidelberg Biosciences International Graduate School (HBIGS). This work was supported by a grant of the Deutsche Forschungsgemeinschaft (MO970/7-1) to A.M. We acknowledge access to the infrastructure of the Cryo-EM Network

at the Heidelberg University (HDcryoNET). J.H. gratefully acknowledges the European Molecular Biology Laboratory (EMBL) for support. This work was supported by a grant of the Deutsche Forschungsgemeinschaft (MO970/7-1) to A.M.

Competing interests

The authors declare that they have no competing interests.

Author contributions

Conceptualization, V.B. J.H. and A.M.
Methodology, V.B, N.M.H., T.M., B.S., D.F., J.H. and A.M.
Investigation, V.B., N.M.H., T.M., P.K., L.M., D.F., J.H. and A.M.
Formal Analysis, V.B., N.M.H., T.M., P.K., L.M., B.S., D.F., I.S., J.H. and A.M.
Resources, P.K. and A.M.
Writing – Original Draft, A.M.
Writing – Review and Editing, V.B., N.M.H., I.S., J.H.
Supervision, A.M., J.H.
Visualization, V.B., J.H., A.M.
Funding Acquisition, A.M.

Data availability section

All data are contained within the manuscript. The NMR structure of ClpL NTD has been deposited at BMRB (accession code 52068)

References

Ahlner A, Carlsson M, Jonsson BH, Lundstrom P (2013) PINT: a software for integration of peak volumes and extraction of relaxation rates. *J Biomol NMR* 56: 191-202

Bogatyreva NS, Finkelstein AV, Galzitskaya OV (2006) Trend of amino acid composition of proteins of different taxa. *J Bioinform Comput Biol* 4: 597-608

Bojer MS, Struve C, Ingmer H, Hansen DS, Krogfelt KA (2010) Heat resistance mediated by a new plasmid encoded Clp ATPase, ClpK, as a possible novel mechanism for nosocomial persistence of Klebsiella pneumoniae. *PLoS One* 5: e15467

Boll EJ, Marti R, Hasman H, Overballe-Petersen S, Stegger M, Ng K, Knochel S, Krogfelt KA, Hummerjohann J, Struve C (2017) Turn Up the Heat-Food and Clinical Escherichia coli Isolates Feature Two Transferrable Loci of Heat Resistance. *Front Microbiol* 8: 579

Bucur FI, Grigore-Gurgu L, Crauwels P, Riedel CU, Nicolau AI (2018) Resistance of Listeria monocytogenes to Stress Conditions Encountered in Food and Food Processing Environments. *Front Microbiol* 9: 2700

Cupo RR, Rizo AN, Braun GA, Tse E, Chuang E, Gupta K, Southworth DR, Shorter J (2022) Unique structural features govern the activity of a human mitochondrial AAA+ disaggregase, Skd3. *Cell Rep* 40: 111408

Delaglio F, Grzesiek S, Vuister GW, Zhu G, Pfeifer J, Bax A (1995) NMRPipe: a multidimensional spectral processing system based on UNIX pipes. *J Biomol NMR* 6: 277-293

Deville C, Carroni M, Franke KB, Topf M, Bukau B, Mogk A, Saibil HR (2017) Structural pathway of regulated substrate transfer and threading through an Hsp100 disaggregase. *Sci Adv* 3: e1701726

Gao H, Li F, Ji Z, Shi Z, Li Y, Yu H (2022) Cryo-EM structures of human p97 double hexamer capture potentiated ATPase-competent state. *Cell Discov* 8: 19

Gasse L, Flemming D, Hurt E (2015) Coordinated Ribosomal ITS2 RNA Processing by the Las1 Complex Integrating Endonuclease, Polynucleotide Kinase, and Exonuclease Activities. *Mol Cell* 60: 808-815

Gupta A, Lentzsch AM, Siegel A, Yu Z, Chio US, Cheng Y, Shan SO (2023) Dodecamer assembly of a metazoan AAA(+) chaperone couples substrate extraction to refolding. *Sci Adv* 9: eadf5336

Haslberger T, Zdanowicz A, Brand I, Kirstein J, Turgay K, Mogk A, Bukau B (2008) Protein disaggregation by the AAA+ chaperone ClpB involves partial threading of looped polypeptide segments. *Nat Struct Mol Biol* 15: 641-650

Huang DC, Huang XF, Novel G, Novel M (1993) Two genes present on a transposon-like structure in Lactococcus lactis are involved in a Clp-family proteolytic activity. *Mol Microbiol* 7: 957-965

Jiang X, Yu T, Liang Y, Ji S, Guo X, Ma J, Zhou L (2016) Efflux pump-mediated benzalkonium chloride resistance in Listeria monocytogenes isolated from retail food. *Int J Food Microbiol* 217: 141-145

Jumper J, Evans R, Pritzel A, Green T, Figurnov M, Ronneberger O, Tunyasuvunakool K, Bates R, Zidek A, Potapenko A *et al* (2021) Highly accurate protein structure prediction with AlphaFold. *Nature* 596: 583-589

Kamal SM, Cimdins-Ahne A, Lee C, Li F, Martin-Rodriguez AJ, Seferbekova Z, Afasizhev R, Wami HT, Katikaridis P, Meins L *et al* (2021a) A recently isolated human commensal Escherichia coli ST10 clone member mediates enhanced thermotolerance and tetrathionate respiration on a P1 phage-derived IncY plasmid. *Mol Microbiol* 115: 255-271

Kamal SM, Simpson DJ, Wang Z, Ganzle M, Romling U (2021b) Horizontal Transmission of Stress Resistance Genes Shape the Ecology of Beta- and Gamma-Proteobacteria. *Front Microbiol* 12: 696522

Katikaridis P, Meins L, Kamal SM, Romling U, Mogk A (2019) ClpG Provides Increased Heat Resistance by Acting as Superior Disaggregase. *Biomolecules* 9

Katikaridis P, Simon B, Jenne T, Moon S, Lee C, Hennig J, Mogk A (2023) Structural basis of aggregate binding by the AAA+ disaggregase ClpG. *bioRxiv*

Kim G, Lee SG, Han S, Jung J, Jeong HS, Hyun JK, Rhee DK, Kim HM, Lee S (2020) ClpL is a functionally active tetradecameric AAA+ chaperone, distinct from hexameric/dodecameric ones. *FASEB J* 34: 14353-14370

Kirstein J, Moliere N, Dougan DA, Turgay K (2009) Adapting the machine: adaptor proteins for Hsp100/Clp and AAA+ proteases. *Nature reviews Microbiology* 7: 589-599

Kriehuber T, Rattei T, Weinmaier T, Bepperling A, Haslbeck M, Buchner J (2010) Independent evolution of the core domain and its flanking sequences in small heat shock proteins. *FASEB J* 24: 3633-3642

Kwon HY, Kim SW, Choi MH, Ogunniyi AD, Paton JC, Park SH, Pyo SN, Rhee DK (2003) Effect of heat shock and mutations in ClpL and ClpP on virulence gene expression in Streptococcus pneumoniae. *Infect Immun* 71: 3757-3765

Lebrun M, Audurier A, Cossart P (1994) Plasmid-borne cadmium resistance genes in Listeria monocytogenes are similar to cadA and cadC of Staphylococcus aureus and are induced by cadmium. *J Bacteriol* 176: 3040-3048

Lee C, Franke KB, Kamal SM, Kim H, Lunsdorf H, Jager J, Nimtz M, Trcek J, Jansch L, Bukau B *et al* (2018) Stand-alone ClpG disaggregase confers superior heat tolerance to bacteria. *Proc Natl Acad Sci U S A* 115: E273-E282

Lee S, Lee SB, Sung N, Xu WW, Chang C, Kim HE, Catic A, Tsai FTF (2023) Structural basis of impaired disaggregase function in the oxidation-sensitive SKD3 mutant causing 3-methylglutaconic aciduria. *Nature communications* 14: 2028

Lee W, Tonelli M, Markley JL (2015) NMRFAM-SPARKY: enhanced software for biomolecular NMR spectroscopy. *Bioinformatics* 31: 1325-1327

Li JS, Bi YT, Dong C, Yang JF, Liang WD (2011) Transcriptome analysis of adaptive heat shock response of Streptococcus thermophilus. *PLoS One* 6: e25777

Lipinska N, Zietkiewicz S, Sobczak A, Jurczyk A, Potocki W, Morawiec E, Wawrzycka A, Gumowski K, Slusarz M, Rodziewicz-Motowidlo S *et al* (2013) Disruption of ionic interactions between the nucleotide binding domain 1 (NBD1) and middle (M) domain in Hsp100 disaggregase unleashes toxic hyperactivity and partial independence from Hsp70. *J Biol Chem* 288: 2857-2869

Liu X, Wang HW (2011) Single particle electron microscopy reconstruction of the exosome complex using the random conical tilt method. *J Vis Exp*

Lunden J, Tolvanen R, Korkeala H (2008) Acid and heat tolerance of persistent and nonpersistent Listeria monocytogenes food plant strains. *Lett Appl Microbiol* 46: 276-280

Maurer M, Linder D, Franke KB, Jager J, Taylor G, Gloge F, Gremer S, Le Breton L, Mayer MP, Weber-Ban E *et al* (2019) Toxic Activation of an AAA+ Protease by the Antibacterial Drug Cyclomarin A. *Cell Chem Biol* 26: 1169-1179 e1164

Mirdita M, Schutze K, Moriwaki Y, Heo L, Ovchinnikov S, Steinegger M (2022) ColabFold: making protein folding accessible to all. *Nat Methods* 19: 679-682

Mogk A, Tomoyasu T, Goloubinoff P, Rüdiger S, Röder D, Langen H, Bukau B (1999) Identification of thermolabile *E. coli* proteins: prevention and reversion of aggregation by DnaK and ClpB. *EMBO J* 18: 6934-6949

Morreale FE, Kleine S, Leodolter J, Junker S, Hoi DM, Ovchinnikov S, Okun A, Kley J, Kurzbauer R, Junk L *et al* (2022) BacPROTACs mediate targeted protein degradation in bacteria. *Cell* 185: 2338-2353 e2318

Naditz AL, Dzieciol M, Wagner M, Schmitz-Esser S (2019) Plasmids contribute to food processing environment-associated stress survival in three Listeria monocytogenes ST121, ST8, and ST5 strains. *Int J Food Microbiol* 299: 39-46

Niklasson M, Otten R, Ahlner A, Andresen C, Schlagnitweit J, Petzold K, Lundstrom P (2017) Comprehensive analysis of NMR data using advanced line shape fitting. *J Biomol NMR* 69: 93-99

Oguchi Y, Kummer E, Seyffer F, Berynskyy M, Anstett B, Zahn R, Wade RC, Mogk A, Bukau B (2012) A tightly regulated molecular toggle controls AAA+ disaggregase. *Nat Struct Mol Biol* 19: 1338-1346

Palleros DR, Reid KL, McCarty JS, Walker GC, Fink AL (1992) DnaK, hsp73, and their molten globules. Two different ways heat shock proteins respond to heat. *J Biol Chem* 267: 5279-5285

Park SS, Kwon HY, Tran TD, Choi MH, Jung SH, Lee S, Briles DE, Rhee DK (2015) ClpL is a chaperone without auxiliary factors. *FEBS J* 282: 1352-1367

Parra-Flores J, Holy O, Bustamante F, Lepuschitz S, Pietzka A, Contreras-Fernandez A, Castillo C, Ovalle C, Alarcon-Lavin MP, Cruz-Cordova A *et al* (2021) Virulence and Antibiotic Resistance Genes in Listeria monocytogenes Strains Isolated From Ready-to-Eat Foods in Chile. *Front Microbiol* 12: 796040

Pontinen A, Aalto-Araneda M, Lindstrom M, Korkeala H (2017) Heat Resistance Mediated by pLM58 Plasmid-Borne ClpL in Listeria monocytogenes. *mSphere* 2

Poyart-Salmeron C, Carlier C, Trieu-Cuot P, Courtieu AL, Courvalin P (1990) Transferable plasmid-mediated antibiotic resistance in Listeria monocytogenes. *Lancet* 335: 1422-1426

Puchades C, Sandate CR, Lander GC (2020) The molecular principles governing the activity and functional diversity of AAA+ proteins. *Nat Rev Mol Cell Biol* 21: 43-58

Ramadan H, Al-Ashmawy M, Soliman AM, Elbediwi M, Sabeq I, Yousef M, Algammal AM, Hiott LM, Berrang ME, Frye JG *et al* (2023) Whole-genome sequencing of Listeria innocua recovered from retail milk and dairy products in Egypt. *Front Microbiol* 14: 1160244

Sattler M, Schleucher J, Griesinger C (1999) Heteronuclear multidimensional NMR experiments for the structure determination of proteins in solution employing pulsed field gradients. *Progress in Nuclear Magnetic Resonance Spectroscopy* 34: 93–158

Seyffer F, Kummer E, Oguchi Y, Winkler J, Kumar M, Zahn R, Sourjik V, Bukau B, Mogk A (2012) Hsp70 proteins bind Hsp100 regulatory M domains to activate AAA+ disaggregase at aggregate surfaces. *Nat Struct Mol Biol* 19: 1347-1355

Shrivastava A, Sandhof CA, Reinle K, Jawed A, Ruger-Herreros C, Schwarz D, Creamer D, Nussbaum-Krammer C, Mogk A, Bukau B (2022) The cytoprotective sequestration activity of small heat shock proteins is evolutionarily conserved. *J Cell Biol* 221

Simon B, Kostler H (2019) Improving the sensitivity of FT-NMR spectroscopy by apodization weighted sampling. *J Biomol NMR* 73: 155-165

Spaulding Z, Thevarajan I, Schrag LG, Zubcevic L, Zolkiewska A, Zolkiewski M (2022) Human mitochondrial AAA+ ATPase SKD3/CLPB assembles into nucleotide-stabilized dodecamers. *Biochem Biophys Res Commun* 602: 21-26

Suokko A, Poutanen M, Savijoki K, Kalkkinen N, Varmanen P (2008) ClpL is essential for induction of thermotolerance and is potentially part of the HrcA regulon in Lactobacillus gasseri. *Proteomics* 8: 1029-1041

Suokko A, Savijoki K, Malinen E, Palva A, Varmanen P (2005) Characterization of a mobile clpL gene from Lactobacillus rhamnosus. *Appl Environ Microbiol* 71: 2061-2069

Tang M, Bruck I, Eritja R, Turner J, Frank EG, Woodgate R, O'Donnell M, Goodman MF (1998) Biochemical basis of SOS-induced mutagenesis in Escherichia coli: reconstitution of in vitro lesion bypass dependent on the UmuD'2C mutagenic complex and RecA protein. *Proc Natl Acad Sci U S A* 95: 9755-9760

Tao L, Biswas I (2013) ClpL is required for folding of CtsR in Streptococcus mutans. *J Bacteriol* 195: 576-584

Taylor G, Frommherz Y, Katikaridis P, Layer D, Sinning I, Carroni M, Weber-Ban E, Mogk A (2022) Antibacterial peptide CyclomarinA creates toxicity by deregulating the Mycobacterium tuberculosis ClpC1-ClpP1P2 protease. *J Biol Chem* 298: 102202

van Heel M, Harauz G, Orlova EV, Schmidt R, Schatz M (1996) A new generation of the IMAGIC image processing system. *J Struct Biol* 116: 17-24

Vieux EF, Wohlever ML, Chen JZ, Sauer RT, Baker TA (2013) Distinct quaternary structures of the AAA+ Lon protease control substrate degradation. *Proc Natl Acad Sci U S A* 110: E2002-2008

Weibezahn J, Tessarz P, Schlieker C, Zahn R, Maglica Z, Lee S, Zentgraf H, Weber-Ban EU, Dougan DA, Tsai FT *et al* (2004) Thermotolerance Requires Refolding of Aggregated Proteins by Substrate Translocation through the Central Pore of ClpB. *Cell* 119: 653-665

Werbeck ND, Schlee S, Reinstein J (2008) Coupling and dynamics of subunits in the hexameric AAA+ chaperone ClpB. *J Mol Biol* 378: 178-190

Winkler J, Tyedmers J, Bukau B, Mogk A (2012) Hsp70 targets Hsp100 chaperones to substrates for protein disaggregation and prion fragmentation. *J Cell Biol* 198: 387-404

Wishart DS, Sykes BD (1994) The 13C chemical-shift index: a simple method for the identification of protein secondary structure using 13C chemical-shift data. *J Biomol NMR* 4: 171-180

Wu D, Liu Y, Dai Y, Wang G, Lu G, Chen Y, Li N, Lin J, Gao N (2023) Comprehensive structural characterization of the human AAA+ disaggregase CLPB in the apo- and substrate-bound states reveals a unique mode of action driven by oligomerization. *PLoS Biol* 21: e3001987

Zolkiewski M (1999) ClpB cooperates with DnaK, DnaJ, and GrpE in suppressing protein aggregation. A novel multi-chaperone system from *Escherichia coli*. *J Biol Chem* 274: 28083-28086

Figure legends

Figure 1

ClpL is an autonomous disaggregase. (A) Domain organizations of ClpL, ClpG, ClpB. All AAA+ proteins consist of two AAA domains (AAA1, AAA2), a coiled-coil middle-domain (M) and diverse N-terminal domains (N). ClpG additionally harbors a disordered C-terminal extension (CTE). (B) Luciferase disaggregation activity (% refolding of aggregated Luciferase/min) of *Lm* ClpL was determined (left). Relative Luciferase disaggregation activities of indicated disaggregation systems were determined (right). KJE: DnaK/DnaJ/GrpE. The disaggregation activity of *Lm* ClpL was set to 1. (C) GFP disaggregation activities (% refolding of aggregated GFP/min) of indicated disaggregation systems were determined. (D) Occurrence of ClpB and ClpL disaggregases in selected Gram-positive bacteria. Loss of heat resistance upon *clpL* deletion in bacteria harboring solely ClpL is indicated. n.d.: not determined. (E) Relative Luciferase and MDH disaggregation activities of *L. gasseri* (*Lg*) ClpL. Disaggregation activities of *Lm* ClpL were set to 1. Standard deviations are based on at least three independent experiments (B,C,E).

Figure 2

Specific molecular features separate ClpL from ClpB/DnaK. (A) Incubation of Luciferase-YFP at 46°C only leads to unfolding of the Luciferase moiety and the formation of mixed aggregates including folded YFP. Unfolding of YFP during disaggregation of aggregated Luciferase-YFP reports on threading power. (B) Aggregated Luciferase-YFP was incubated in presence of indicated disaggregation machineries and YFP fluorescence was recorded. Initial YFP fluorescence was set at 100%. (C/D) Melting temperatures of ClpL, *Lm* ClpB and *Lm* DnaK were determined in presence of indicated nucleotides by SYPRO®Orange binding (C) or nanoDSF (D). Standard deviations are based on at least three independent experiments (C,D).

Figure 3

The ClpL NTD is essential for disaggregation activity. (A) Disaggregation activities of ClpL and ClpL-ΔN towards aggregated Luciferase and MDH (each: % regain enzymatic activity/min) were determined. The activity of ClpL was set to 1. (B) ATPase activities of ClpL and ClpL-ΔN were determined. The ATPase activity of ClpL was set to 1. (C) *E. coli* Δ*clpB* cells harboring plasmids for constitutive expression of Luciferase and IPTG-controlled expression of indicated disaggregases were grown at 30°C to mid-logarithmic growth phase and heat shocked to 46°C for 15 min. Luciferase activities prior to heat shock were set to 100%. The regain of Luciferase activity was determined after a 120 min recovery period at 30°C. 10/100/500: μM IPTG added to induce disaggregase expression. p: empty vector control. (D) *E. coli* Δ*clpB* cells harboring plasmids for expression of indicated disaggregases were grown at 30°C to mid-logarithmic growth phase and shifted to 49°C. Serial dilutions of cells were prepared at the indicated time points, spotted on LB plates and incubated at 30°C. 10/100/500: μM IPTG added to induce disaggregase expression. p: empty vector control. (E) Domain organization of the ClpL-ClpB chimera L_N-ClpB*. ClpB* harbors the K476C mutation in its M-domain, abrogating ATPase repression. (F) Luciferase disaggregation activities (% refolded Luciferase/min) of indicated disaggregation machineries were determined. The disaggregation activity of ClpL was set to 1. Standard deviations are based on at least three independent experiments (A,B,C,F).

Figure 4

Molecular basis of ClpL NTD binding to protein aggregates. (A) AlphaFold2 model of ClpL NTD. The colour code depicts the calculated confidence of the prediction (pLDDT). Residues that potentially participate in the formation of small hydrophobic cores (α1/2 (cyan) and α2/β1,2 (magenta)) are indicated. (B) Secondary structure of ClpL-NTD as determined by NMR using secondary chemical shifts (Cα, Cβ). Secondary structure elements determined from NMR and from the AlphaFold prediction are indicated below the histogram. The predicted α1-helix only transiently forms in isolated solution context, which is confirmed by further NMR analysis (Fig. S5E). (C) Composition of ClpL NTDs. The frequencies (%) of individual amino acids represent the ratio of the number of a particular residue and the total length of respective NTDs (*L. monocytogenes, Staphylococcus aureus, S. pneumoniae, Lactobacillus plantarum, Oenococcus oeni, Lactobacillus rhamnosus, Streptococcus suis*). The average frequency of each amino acid in the total bacterial proteomes is given as reference (Bogatyreva *et al*, 2006). (D) Localization of patches A-E, consisting of aromatic and N/Q residues are indicated. (F/G) Luciferase and MDH disaggregation activities (% refolded enzyme/min) of ClpL WT and indicated patch mutants were determined. The disaggregtion activity of ClpL was set to 1. (G) ClpG, ClpL and indicated ClpL mutants were incubated with aggregated MDH in presence of ATPγS. The extend of aggregate binding was determined by co-sedimentation upon centrifugation. Standard deviations are based on at least three independent experiments (E,F,G).

Figure 5

Multiple ClpL NTDs are required for disaggregation activity. (A) Varying the ratio of L_N-ClpB* and ΔN-ClpB* leads to formation of mixed hexamers with diverse numbers of NTDs. (B) Luciferase disaggregation activities (% refolded Luciferase/min) of mixed L_N-ClpB*/ΔN-ClpB* hexamers were determined and compared with curves calculated from a model (black to grey), which assumes that a mixed hexamer only displays disaggregation activity if it contains the number of NTDs indicated. Mixing ratios are indicated as number of ΔN-ClpB* in a hexamer. (C/D) Luciferase disaggregation activities of L_N-ClpB* (C) and ClpL (D) were determined in absence and presence of an excess of isolated NTD as indicated. Disaggregation activities determined in NTD absence were set as 100%. Standard deviations are based on at least three independent experiments (C/D).

Figure 6

Stabilizing ClpL ring dimers strongly reduces disaggregation activity. (A) AlphaFold2 model of *Lm* ClpL ring dimers. Positions of individual domains are indicated. (B) Negative stain EM of *Lm* ClpL. 2D class averages revealing single ring hexamers or heptamers, ring dimers and tetramers of rings are indicated. The scale bar is 100 nm. (C) Populations of diverse ClpL assembly states based on 2D class averages were determined for *Lm* ClpL WT and indicated mutants and *Lg* ClpL. (D) obtained for the WT and the F444S mutant. (D/E) Disaggregation activities of ClpL WT and indicated M-domain (M) mutants towards aggregated Luciferase (D) and MDH (E) (each: % regain enzymatic activity/min) were determined. The activity of ClpL was set to 1. (F) Model of ClpL ring dimers. Positions of T355 residues in interacting M-domains are depicted. Crosslinking of ClpL T355C was achieved by DTT removal and further incubation at RT as indicated. The formation of crosslinked ClpL T355C dimers was monitored by SDS-PAGE and Coomassie-staining. Addition of 10 mM DTT reversed the disulfide bonds. (G) Luciferase disaggregation activities of reduced ClpL WT and oxidized ClpL WT or ClpL T355C were determined in absence of DTT (-DTT). Oxidized variants (WT and T355C) were additionally preincubated with 10 mM DTT for 30 min and tested for disaggregation activity in presence of DTT (+DTT). The factor of increase in disaggregation activity upon reduction (+DTT) is indicated (right). Standard deviations are based on at least three independent

experiments (D/E/G), standard deviations for the activity gain factors have been propagated from disaggregation activity standard deviations.

A

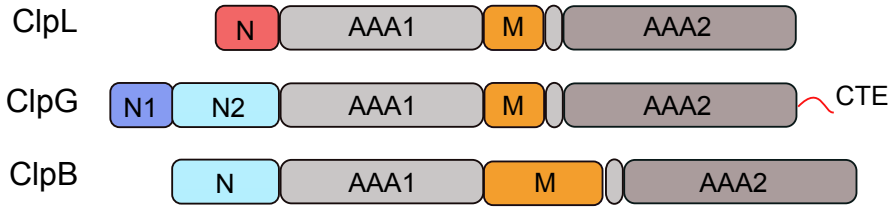

B

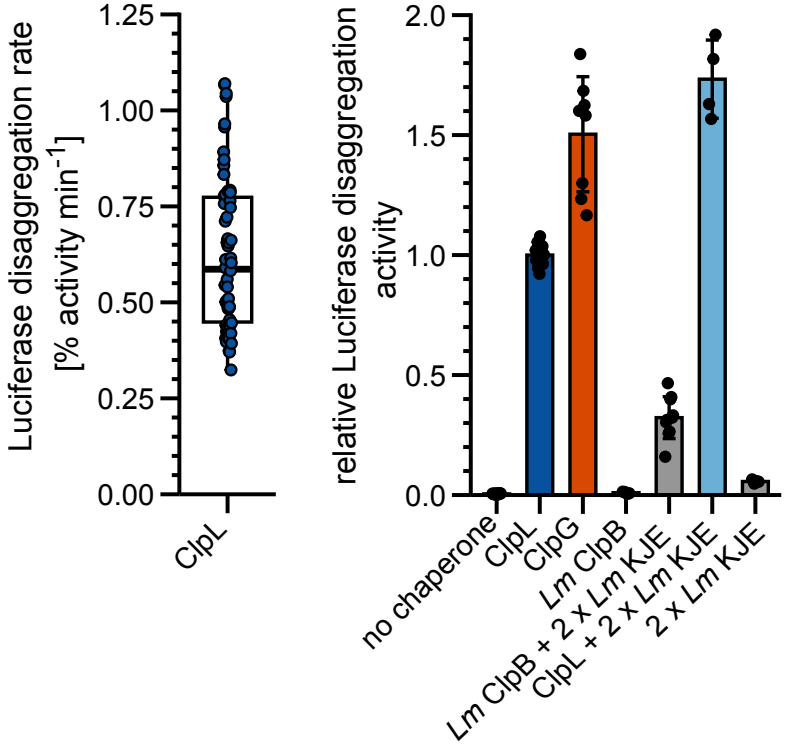

C

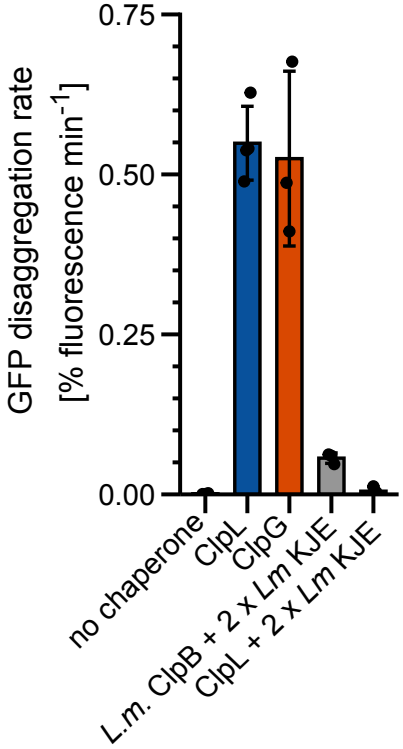

D

	genes present		loss of heat resistance
strain	*clpB*	*clpL*	Δ*clpL*
Lactobacillus rhamnosus	+	+	
Lactobacillus gasseri		+	+
Lactobacillus johnsonii		+	n.d.
Lactobacillus acidophilus		+	n.d.
Lactococcus lactis	+	+	
Leuconostoc mesenteroides		+	
Listeria monocytogenes	+	+	+
Oenococcus oeni		+	n.d.
Staphylococcus aureus	+	+	+
Streptococus pneumoniae	+	+	
Streptococcus thermophilus		+	+

E

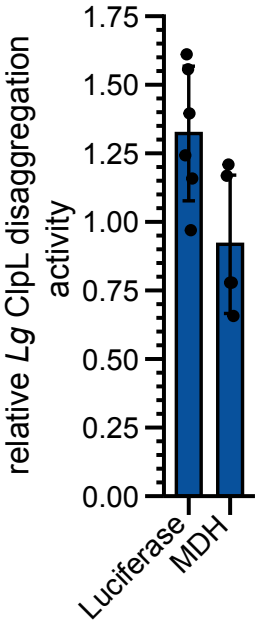

Figure 1

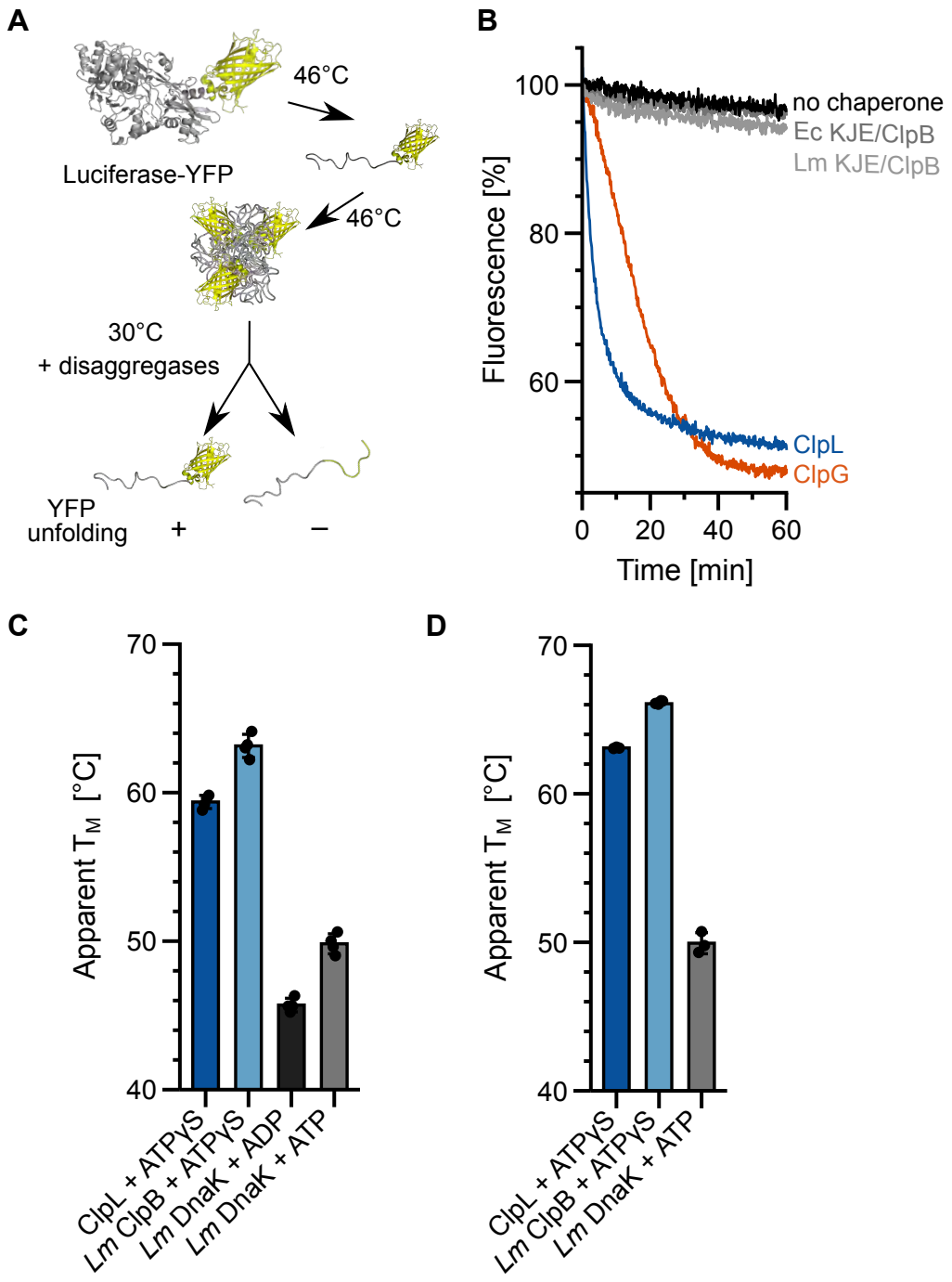
A
46°C
Luciferase-YFP
46°C
30°C
+ disaggregases
YFP
unfolding
+
–
B
100
80
60
Fluorescence [%]
no chaperone
Ec KJE/ClpB
Lm KJE/ClpB
ClpL
ClpG
0
20
40
60
Time [min]
C
70
60
50
40
Apparent T_M [°C]
ClpL + ATPγS
Lm ClpB + ATPγS
Lm DnaK + ADP
Lm DnaK + ATP
D
70
60
50
40
Apparent T_M [°C]
ClpL + ATPγS
Lm ClpB + ATPγS
Lm DnaK + ATP

Figure 2

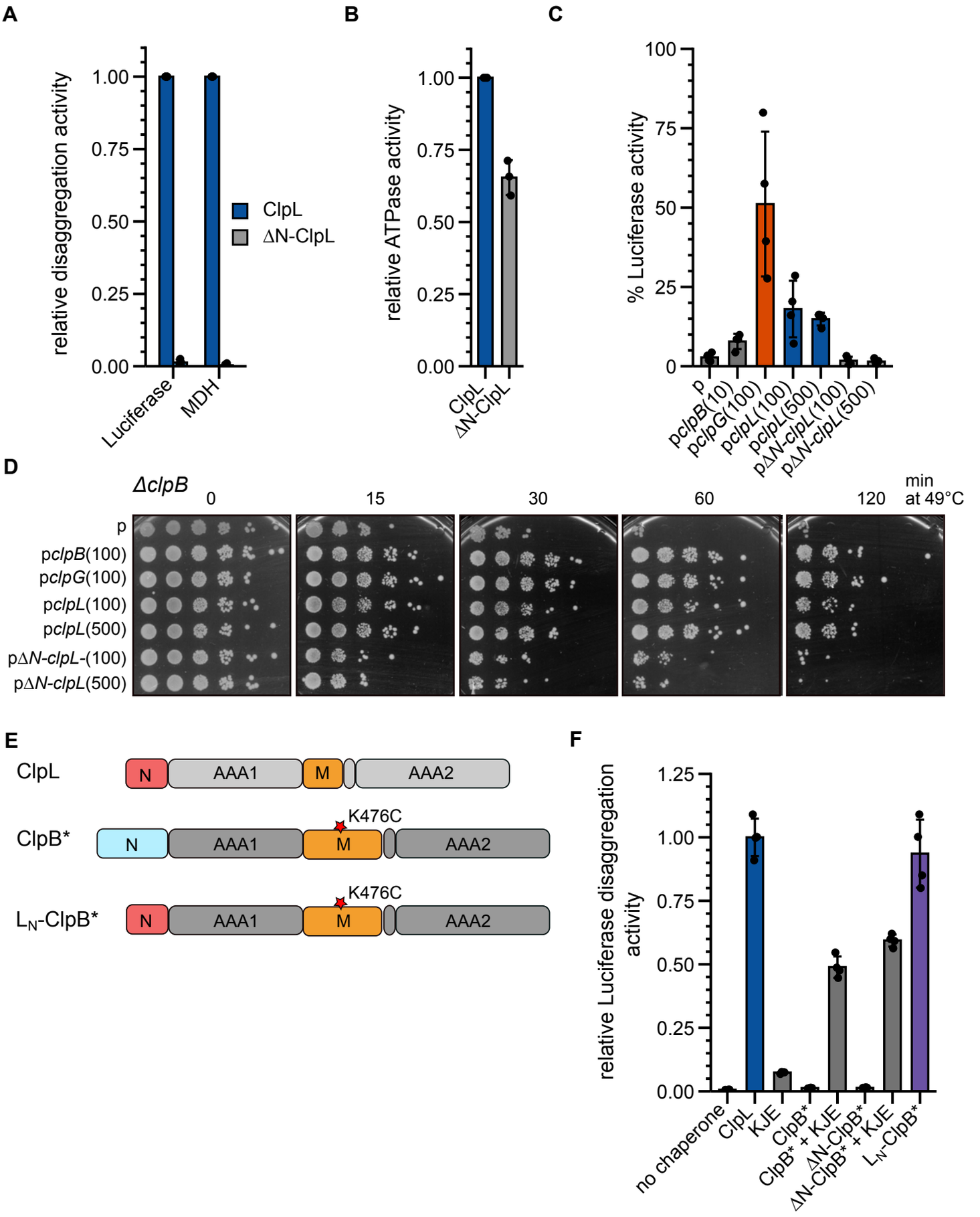
A
relative disaggregation activity
1.00
0.75
0.50
0.25
0.00
ClpL
ΔN-ClpL
Luciferase
MDH
B
relative ATPase activity
1.00
0.75
0.50
0.25
0.00
ClpL
ΔN-ClpL
C
% Luciferase activity
100
75
50
25
0
p
pclpB(10)
pclpG(100)
pclpL(100)
pclpL(500)
pΔN-clpL(100)
pΔN-clpL(500)
D
ΔclpB
0
15
30
60
120
min at 49°C
p
pclpB(100)
pclpG(100)
pclpL(100)
pclpL(500)
pΔN-clpL-(100)
pΔN-clpL(500)
E
ClpL
N
AAA1
M
AAA2
ClpB*
K476C
LN-ClpB*
F
relative Luciferase disaggregation activity
1.25
1.00
0.75
0.50
0.25
0.00
no chaperone
ClpL
KJE
ClpB*
ClpB* + KJE
ΔN-ClpB*
ΔN-ClpB* + KJE
LN-ClpB*

Figure 3

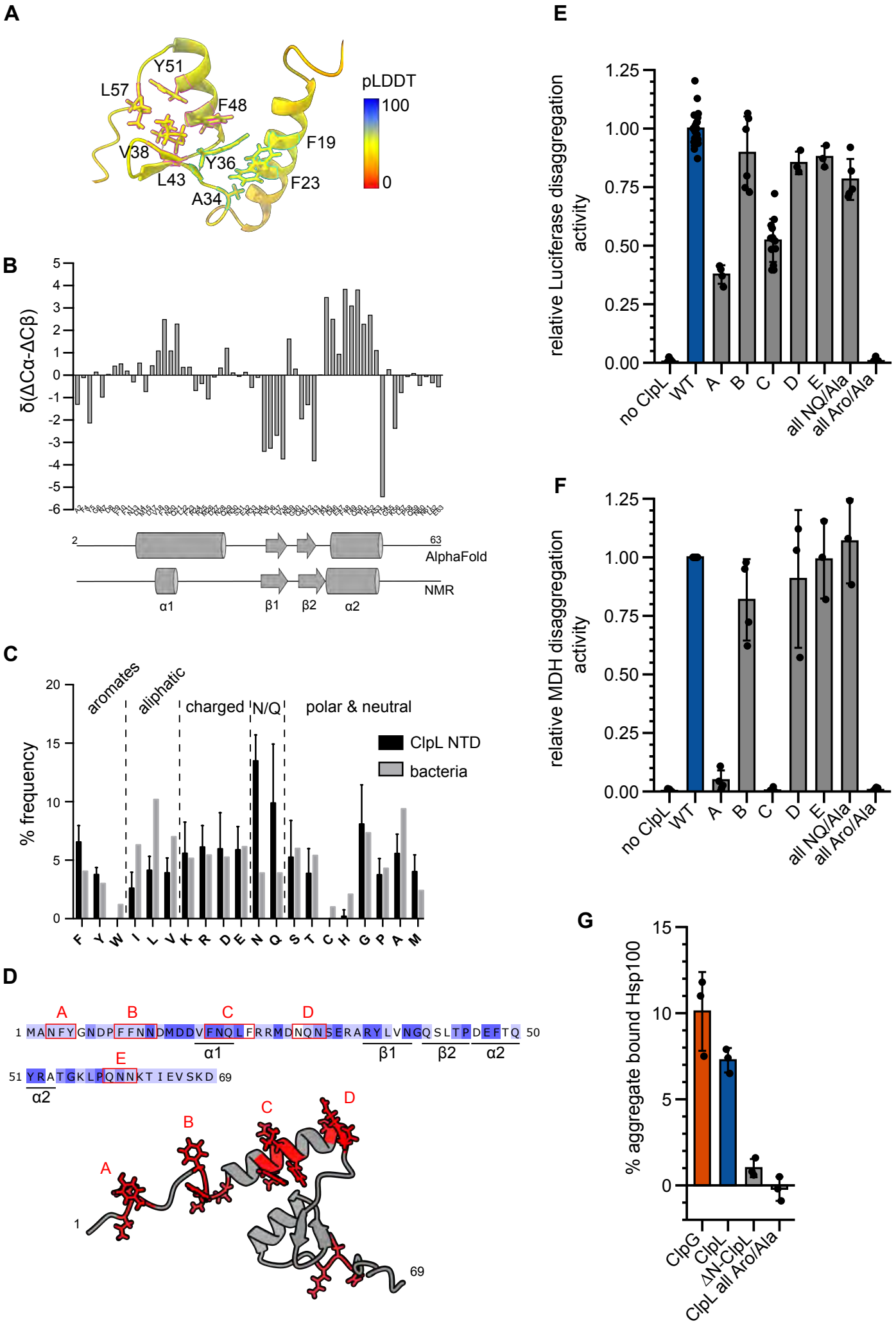
A
Y51
L57
F48
V38
Y36
L43
A34
F19
F23
pLDDT
100
0
B
δ(ΔCα-ΔCβ)
AlphaFold
NMR
α1
β1
β2
α2
C
aromates
aliphatic
charged
N/Q
polar & neutral
ClpL NTD
bacteria
% frequency
D
A
B
C
D
E
α1
β1
β2
α2
E
relative Luciferase disaggregation activity
no ClpL
WT
A
B
C
D
E
all NQ/Ala
all Aro/Ala
F
relative MDH disaggregation activity
G
% aggregate bound Hsp100
ClpG
ClpL
ΔN-ClpL
ClpL all Aro/Ala

Figure 4

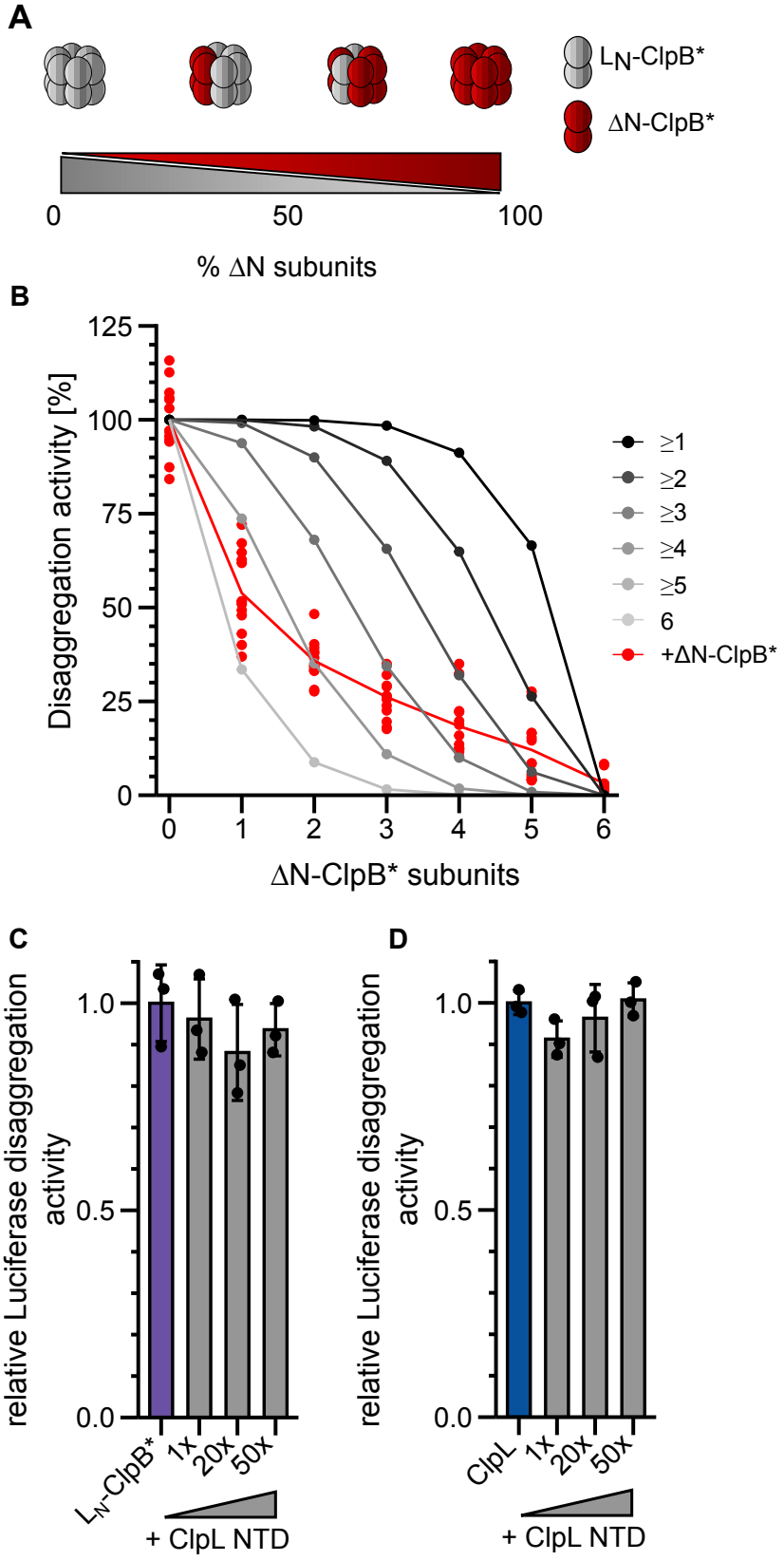
A
LN-ClpB*
ΔN-ClpB*
0
50
100
% ΔN subunits
B
Disaggregation activity [%]
125
100
75
50
25
0
0
1
2
3
4
5
6
ΔN-ClpB* subunits
≥1
≥2
≥3
≥4
≥5
6
+ΔN-ClpB*
C
relative Luciferase disaggregation activity
1.0
0.5
0.0
LN-ClpB*
1x
20x
50x
+ ClpL NTD
D
relative Luciferase disaggregation activity
1.0
0.5
0.0
ClpL
1x
20x
50x
+ ClpL NTD

Figure 5

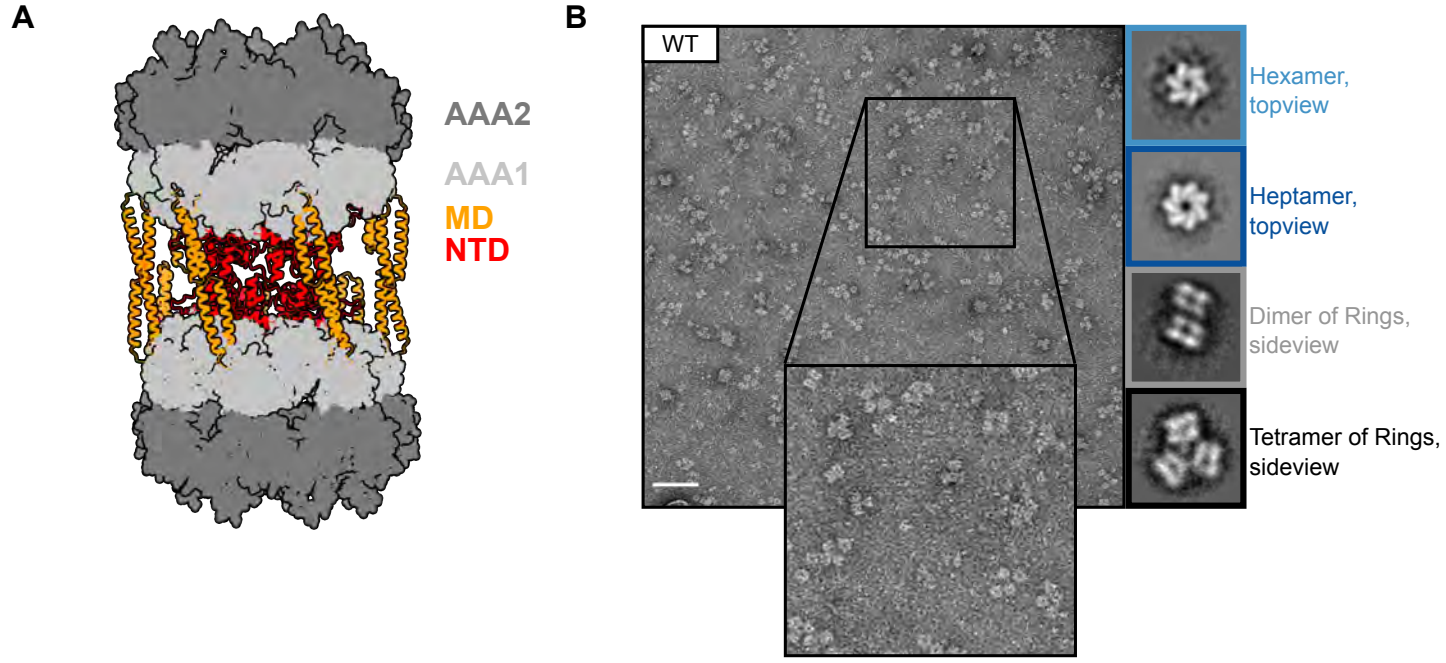
A
AAA2
AAA1
MD
NTD
B
WT
Hexamer, topview
Heptamer, topview
Dimer of Rings, sideview
Tetramer of Rings, sideview

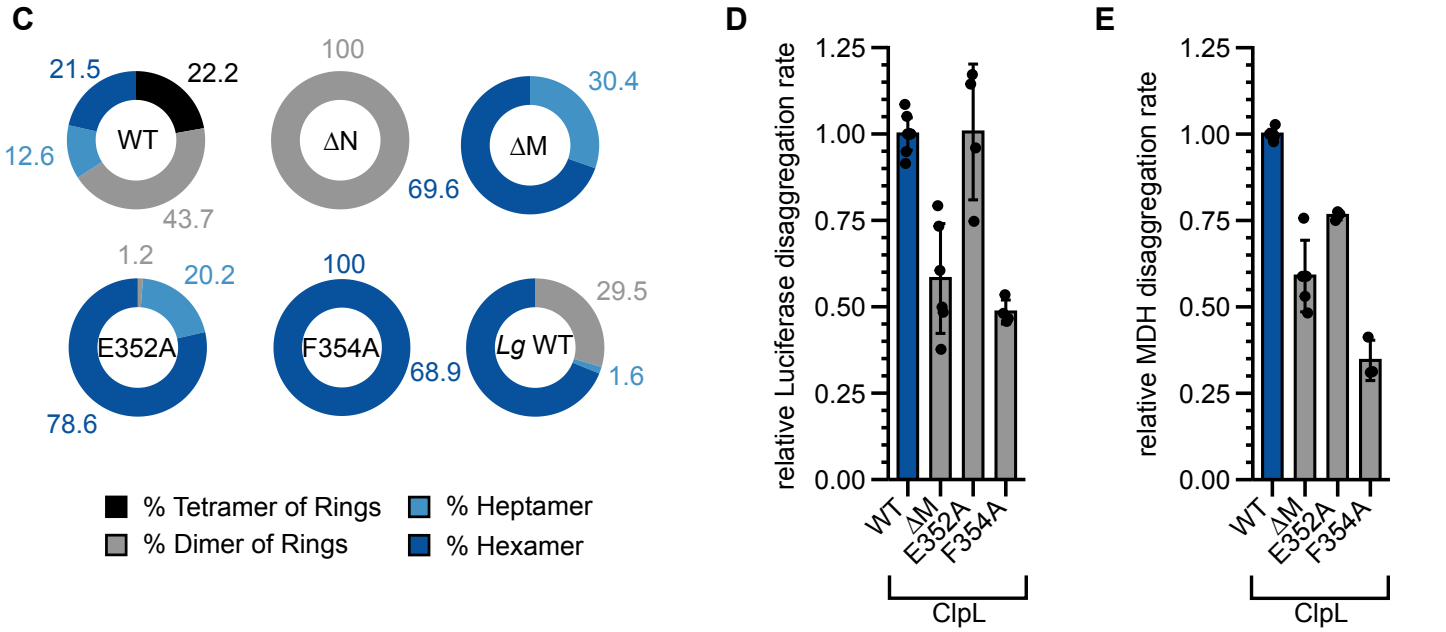
C
WT
21.5
22.2
12.6
43.7
ΔN
100
ΔM
30.4
69.6
E352A
1.2
20.2
78.6
F354A
100
68.9
Lg WT
29.5
1.6
% Tetramer of Rings
% Heptamer
% Dimer of Rings
% Hexamer
D
relative Luciferase disaggregation rate
1.25
1.00
0.75
0.50
0.25
0.00
WT
ΔM
E352A
F354A
ClpL
E
relative MDH disaggregation rate
1.25
1.00
0.75
0.50
0.25
0.00
WT
ΔM
E352A
F354A
ClpL

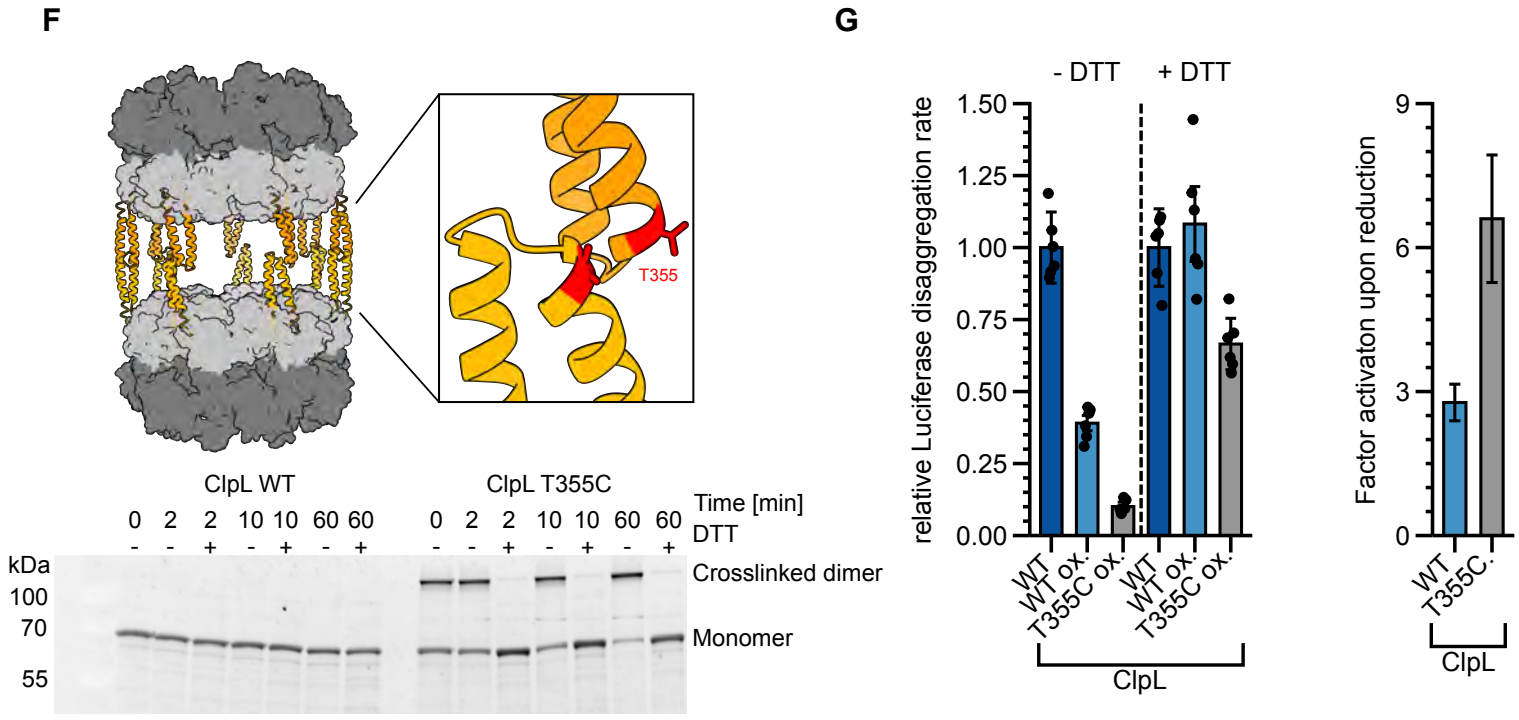
F
T355
ClpL WT
ClpL T355C
Time [min]
0 2 2 10 10 60 60
0 2 2 10 10 60 60
DTT
- - + - + - +
- - + - + - +
kDa
100
70
55
Crosslinked dimer
Monomer
G
- DTT
+ DTT
relative Luciferase disaggregation rate
1.50
1.25
1.00
0.75
0.50
0.25
0.00
WT
WT ox.
T355C ox.
WT
WT ox.
T355C ox.
ClpL
Factor activaton upon reduction
9
6
3
0
WT
T355C.
ClpL

Figure 6

Table S1: strains and plasmids used in this study

Strain	Description	Source or reference
E. coli XL1 blue	*recA1 endA1 gyrA96 thi-1 hsdR1 supE44 relA1 lac* [F' *proAB lacI*^{q} *ΔM15* Tn10 (Tcr)]	Stratagene
E. coli BL21	*F- ompT lon hsdSB gal dcm λ* (DE3)	Novagen
E. coli ΔclpB	MC1000 Δ*clpB*::Km	(1)
E. coli dnak103	MC4100 *dnak103*	(1)
Plasmid	**Description**	**Source or reference**
pET24a-*clpL*	Vector for IPTG-inducible expression of *clpL* in *E.coli* BL21 cells, fused C-terminal 6xHis-tag	This study
pET24a-*clpL-ΔN*	Vector for IPTG-inducible expression of *clpL-ΔN* in *E.coli* BL21 cells, fused C-terminal 6xHis-tag	This study
pET24a-*Lm_clpB*	Vector for IPTG-inducible expression of *Lm clpB* in *E.coli* BL21 cells, fused C-terminal 6xHis-tag	This study
pET24a-*Lm_DnaK*	Vector for IPTG-inducible expression of *Lm_DnaK* in *E.coli* BL21 cells, fused C-terminal 6xHis-tag	This study
pET24a-*Lm_DnaJ*	Vector for IPTG-inducible expression of *Lm_DnaJ* in *E.coli* BL21 cells, fused C-terminal 6xHis-tag	This study
pET24a-*Lm_GrpE*	Vector for IPTG-inducible expression of *Lm_GrpE* in *E.coli* BL21 cells, fused C-terminal 6xHis-tag	This study
pET24a-*clpL-Patch_A*	Vector for IPTG-inducible expression of *clpL-Patch_A* in *E.coli* BL21 cells, fused C-terminal 6xHis-tag	This study
pET24a-*clpL-Patch_B*	Vector for IPTG-inducible expression of *clpL-Patch_B* in *E.coli* BL21 cells, fused C-terminal 6xHis-tag	This study
pET24a-*clpL-Patch_C*	Vector for IPTG-inducible expression of *clpL-Patch_C* in *E.coli* BL21 cells, fused C-terminal 6xHis-tag	This study
pET24a-*clpL-Patch_D*	Vector for IPTG-inducible expression of *clpL-Patch_D* in *E.coli* BL21 cells, fused C-terminal 6xHis-tag	This study
pET24a-*clpL-Patch_E*	Vector for IPTG-inducible expression of *clpL-Patch_E* in *E.coli* BL21 cells, fused C-terminal 6xHis-tag	This study
pET24a-*clpL-Patch_AB*	Vector for IPTG-inducible expression of *clpL-Patch_AB* in *E.coli* BL21 cells, fused C-terminal 6xHis-tag	This study
pET24a-*clpL-Patch_AC*	Vector for IPTG-inducible expression of *clpL-Patch_AC* in *E.coli* BL21 cells, fused C-terminal 6xHis-tag	This study
pET24a-*clpL-Patch_BC*	Vector for IPTG-inducible expression of *clpL-Patch_BC* in *E.coli* BL21 cells, fused C-terminal 6xHis-tag	This study
pET24a-*clpL_all_NQ→Ala*	Vector for IPTG-inducible expression of *clpL-Patch_all_NQ→Ala* in *E.coli* BL21 cells, fused C-terminal 6xHis-tag	This study
pET24a-*clpL-Patch_all_Aro→Ala*	Vector for IPTG-inducible expression of *clpL-Patch_all_Aro→Ala* in *E.coli* BL21 cells, fused C-terminal 6xHis-tag	This study
pET24a-*clpL-Y36A*	Vector for IPTG-inducible expression of *clpL-Y36A* in *E.coli* BL21 cells, fused C-terminal 6xHis-tag	This study
pET24a-*clpL-F48A*	Vector for IPTG-inducible expression of *clpL-F48A* in *E.coli* BL21 cells, fused C-terminal 6xHis-tag	This study
pET24a-*clpL-Y51A*	Vector for IPTG-inducible expression of *clpL-Y51A* in *E.coli* BL21 cells, fused C-terminal 6xHis-tag	This study
pET24a-*clpL-NTD61*	Vector for IPTG-inducible expression of *clpL_NTD61* in *E.coli* BL21 cells, fused C-terminal 6xHis-tag	This study
pET24a-*clpL-NTD78*	Vector for IPTG-inducible expression of *clpL_NTD78* in *E.coli* BL21 cells, fused C-terminal 6xHis-tag	This study
pCA528-*clpL-E352A*	Vector for IPTG-inducible expression of *clpL-E352A* in *E.coli* BL21 cells, fused cleavable N-terminal 6xHis-SUMO-tag	This study
pCA528-*clpL-F354A*	Vector for IPTG-inducible expression of *clpL-F354A* in *E.coli* BL21 cells, fused cleavable N-terminal 6xHis-SUMO-tag	This study
pCA528-*clpL-T355C*	Vector for IPTG-inducible expression of *clpL-T355C* in *E.coli* BL21 cells, fused cleavable N-terminal 6xHis-SUMO-tag	This study
pC6AmpΔBsaI-L_N-*ClpB**	Vector for IPTG-inducible expression of L_N-*ClpB** in *E.coli* BL21 cells, fused cleavable N-terminal 6xHis-SUMO-tag	This study
pC6AmpΔBsaI-L_N-*ClpB*-E199A-E598A*	Vector for IPTG-inducible expression of L_N-*ClpB*- E199A-E598A* in *E.coli* BL21 cells, fused cleavable N-terminal 6xHis-SUMO-tag	This study
pC6AmpΔBsaI-L_N-*ClpB*-Patch_A*	Vector for IPTG-inducible expression of L_N-*ClpB*-Patch_A* in *E.coli* BL21 cells, fused cleavable N-terminal 6xHis-SUMO-tag	This study
pC6AmpΔBsaI-L_N-*ClpB*-Patch_AB*	Vector for IPTG-inducible expression of L_N-*ClpB*-Patch_AB* in *E.coli* BL21 cells, fused cleavable N-terminal 6xHis-SUMO-tag	This study
pC6AmpΔBsaI-L_N-*ClpB*-Patch_C*	Vector for IPTG-inducible expression of L_N-*ClpB*-Patch_C* in *E.coli* BL21 cells, fused cleavable N-terminal 6xHis-SUMO-tag	This study

pC6AmpΔBsaI-L_N-*ClpB*-Y36A*	Vector for IPTG-inducible expression of L_N-*ClpB*-Y36A* in *E.coli* BL21 cells, fused cleavable N-terminal 6xHis-SUMO-tag	This study
pC6AmpΔBsaI-L_N-*ClpB*-F48A*	Vector for IPTG-inducible expression of L_N-*ClpB*-F48A* in *E.coli* BL21 cells, fused cleavable N-terminal 6xHis-SUMO-tag	This study
pC6AmpΔBsaI-L_N-*ClpB*-Y51A*	Vector for IPTG-inducible expression of L_N-*ClpB*-Y51A* in *E.coli* BL21 cells, fused cleavable N-terminal 6xHis-SUMO-tag	This study
pUHE21-2fd12	Empty Vector control for *in vivo* assays	This study
pUHE21-$clpG_{GI}$	Vector for IPTG-inducible expression of $clpG_{GI}$ in *E.coli ΔclpB* cells	adjust
pUHE21-*Ec clpB*	Vector for IPTG-inducible expression of *Ec clpB* in *E.coli ΔclpB* cells	adjust
pDS56-*clpL*	Vector for IPTG-inducible expression of *clpL* in *E.coli* ⍰*clpB* cells and *E. coli dnak103* cells	This study
pUHE21-*clpL-ΔN*	Vector for IPTG-inducible expression of *clpL* in *E.coli* ⍰*clpB* cells and *E. coli dnak103* cells	This study
pUHE21-*Ec* dnaK	Vector for IPTG-inducible expression of *Ec dnaK* in *E.coli dnak103* cells	(1)
pET24a-$clpG_{GI}$	Vector for IPTG-inducible expression of $clpG_{GI}$ in *E.coli* BL21 cells, fused C-terminal 6xHis-tag	adjust
pDS56-*Ec clpB*	Vector for IPTG-inducible expression of *Ec clpB* in *E.coli ΔclpB* cells, fused C-terminal 6xHis-tag	(1)
pUHE21-*Ec dnaK*-His	Vector for IPTG-inducible expression of *Ec dnaK* in *E.coli ΔclpB* cells, fused C-terminal 6xHis-tag	(1)
pCA528-*Ec dnaJ*	Vector for IPTG-inducible expression of *Ec dnaJ* in *E.coli* BL21 cells, fused cleavable N-terminal 6xHis-SUMO-tag	(1)
pCA528-*Ec grpE*	Vector for IPTG-inducible expression of *Ec grpE* in *E.coli* BL21 cells, fused cleavable N-terminal 6xHis-SUMO-tag	(1)
pDS56-*Ec* ΔN-ClpB-K476C	Vector for IPTG-inducible expression of *Ec ΔN-clpB-K476C* in *E.coli ΔclpB* cells, fused C-terminal 6xHis-tag	(2)
pDS56-*luciferase*	Vector for IPTG-inducible expression of *luciferase* in *E.coli ΔclpB* cells, fused N-terminal 6xHis-tag	(3)
pDS56-*luciferase-yfp*	Vector for IPTG-inducible expression of *luciferase-YFP* in *E.coli ΔclpB* cells, fused N-terminal 6xHis-tag	(3)

References

1. Lee, C., Franke, K. B., Kamal, S. M., Kim, H., Lunsdorf, H., Jager, J., Nimtz, M., Trcek, J., Jansch, L., Bukau, B., Mogk, A., and Romling, U. (2018) Stand-alone ClpG disaggregase confers superior heat tolerance to bacteria. *Proc Natl Acad Sci U S A* **115**, E273-E282
2. Oguchi, Y., Kummer, E., Seyffer, F., Berynskyy, M., Anstett, B., Zahn, R., Wade, R. C., Mogk, A., and Bukau, B. (2012) A tightly regulated molecular toggle controls AAA+ disaggregase. *Nat Struct Mol Biol* **19**, 1338-1346
3. Haslberger, T., Zdanowicz, A., Brand, I., Kirstein, J., Turgay, K., Mogk, A., and Bukau, B. (2008) Protein disaggregation by the AAA+ chaperone ClpB involves partial threading of looped polypeptide segments. *Nat Struct Mol Biol* **15**, 641-650

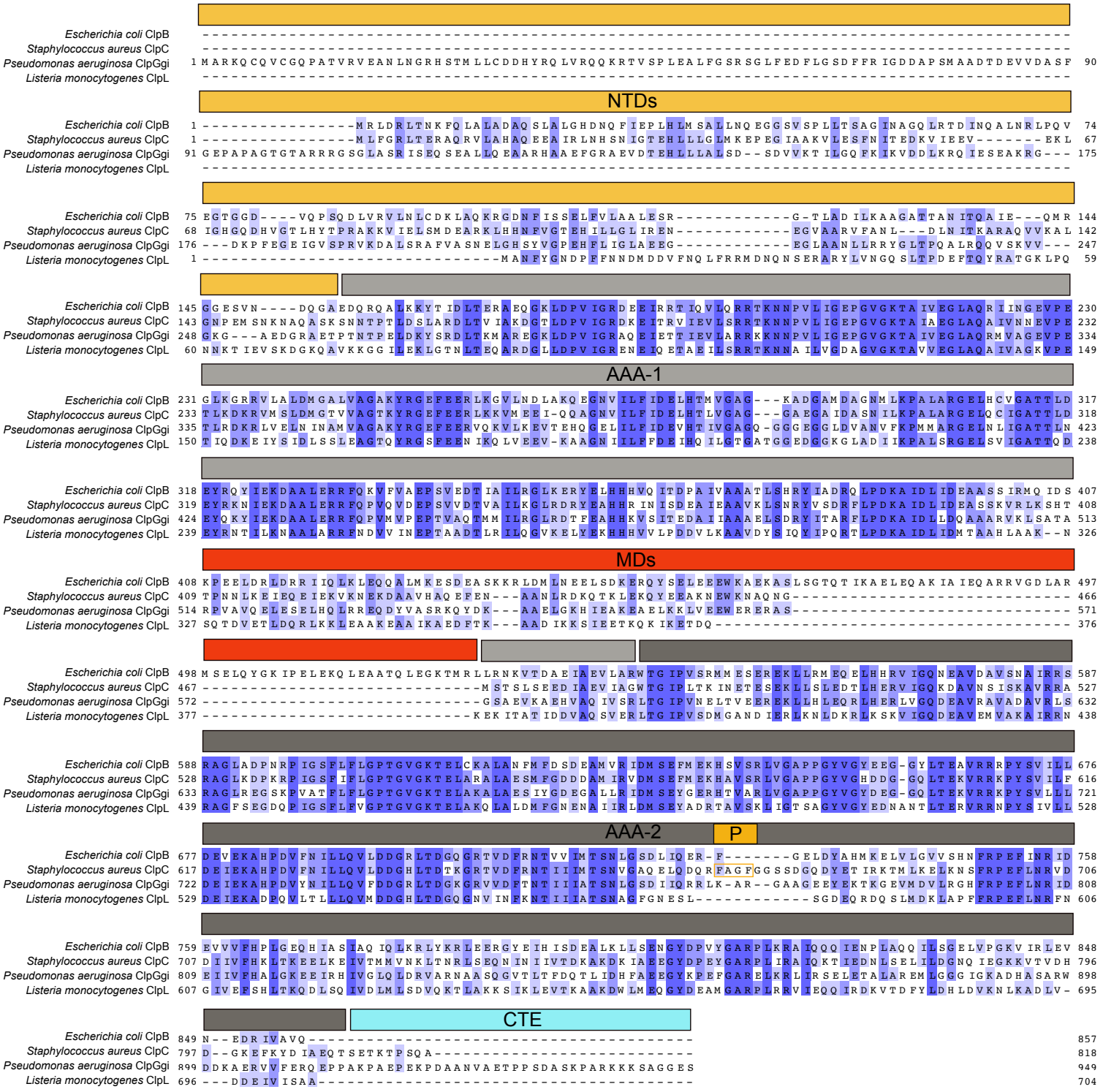

Figure 1 - figure supplement 1

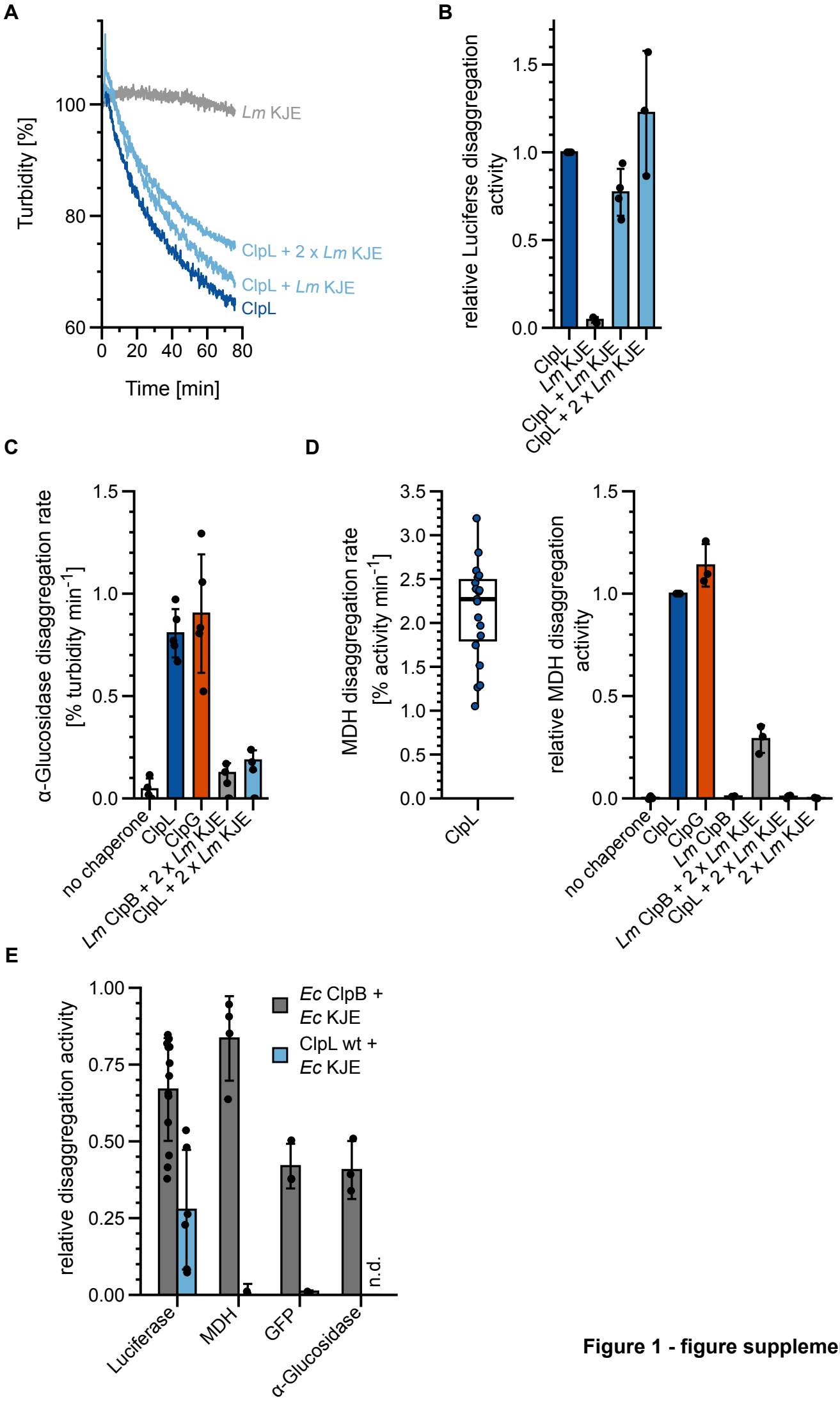

Figure 1 - figure supplement 2

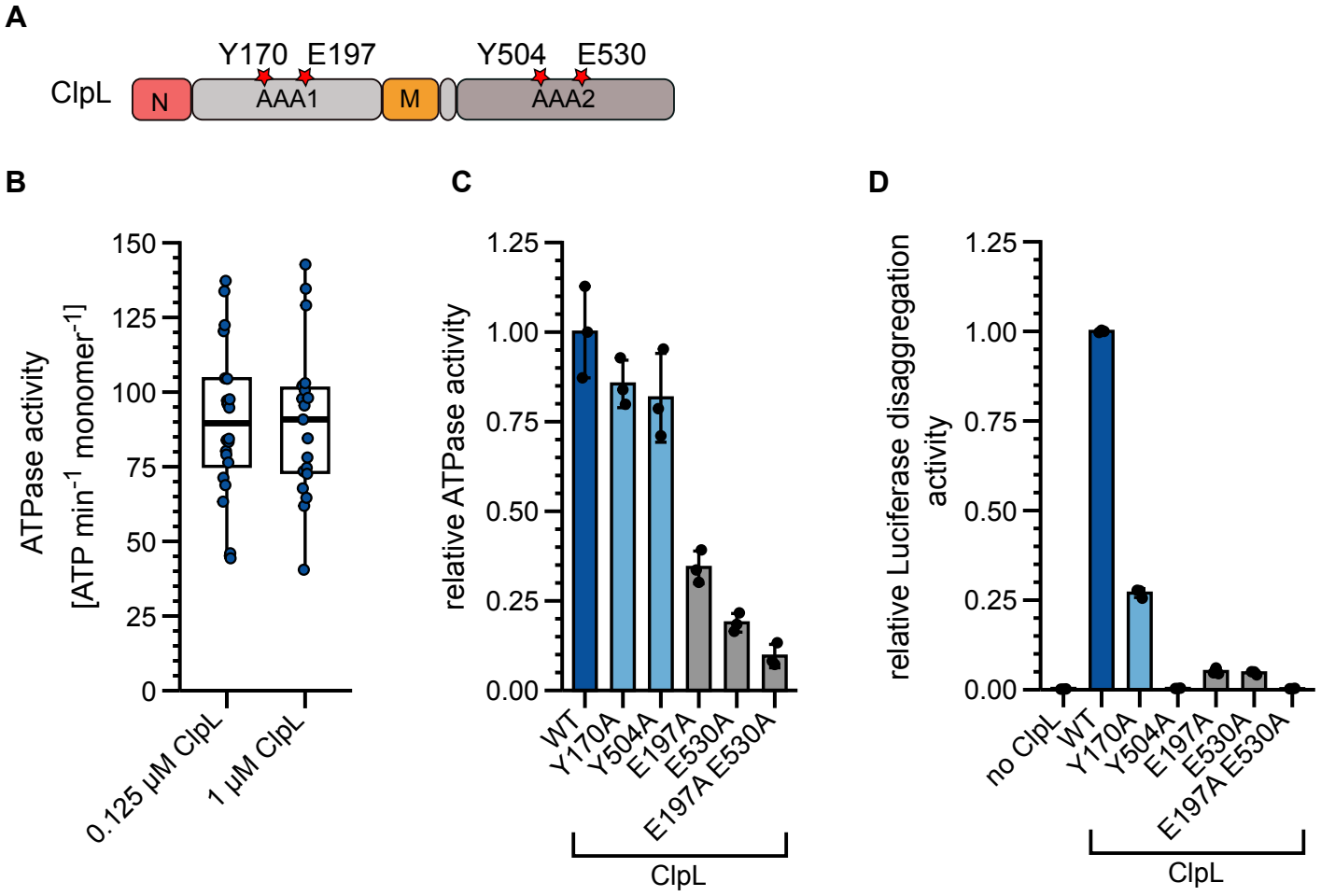

Figure 3 - figure supplement 1

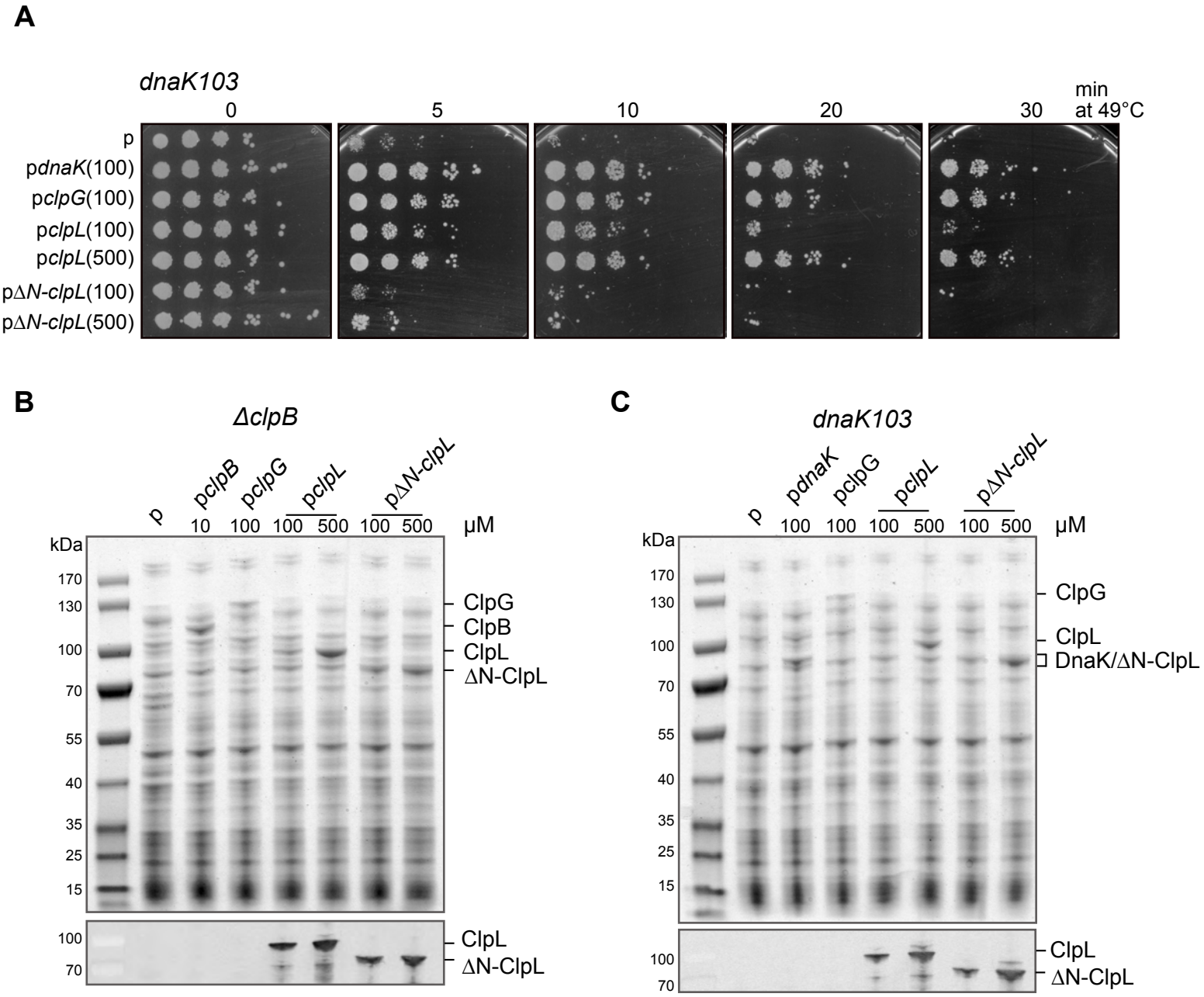

Figure 3 - figure supplement 2

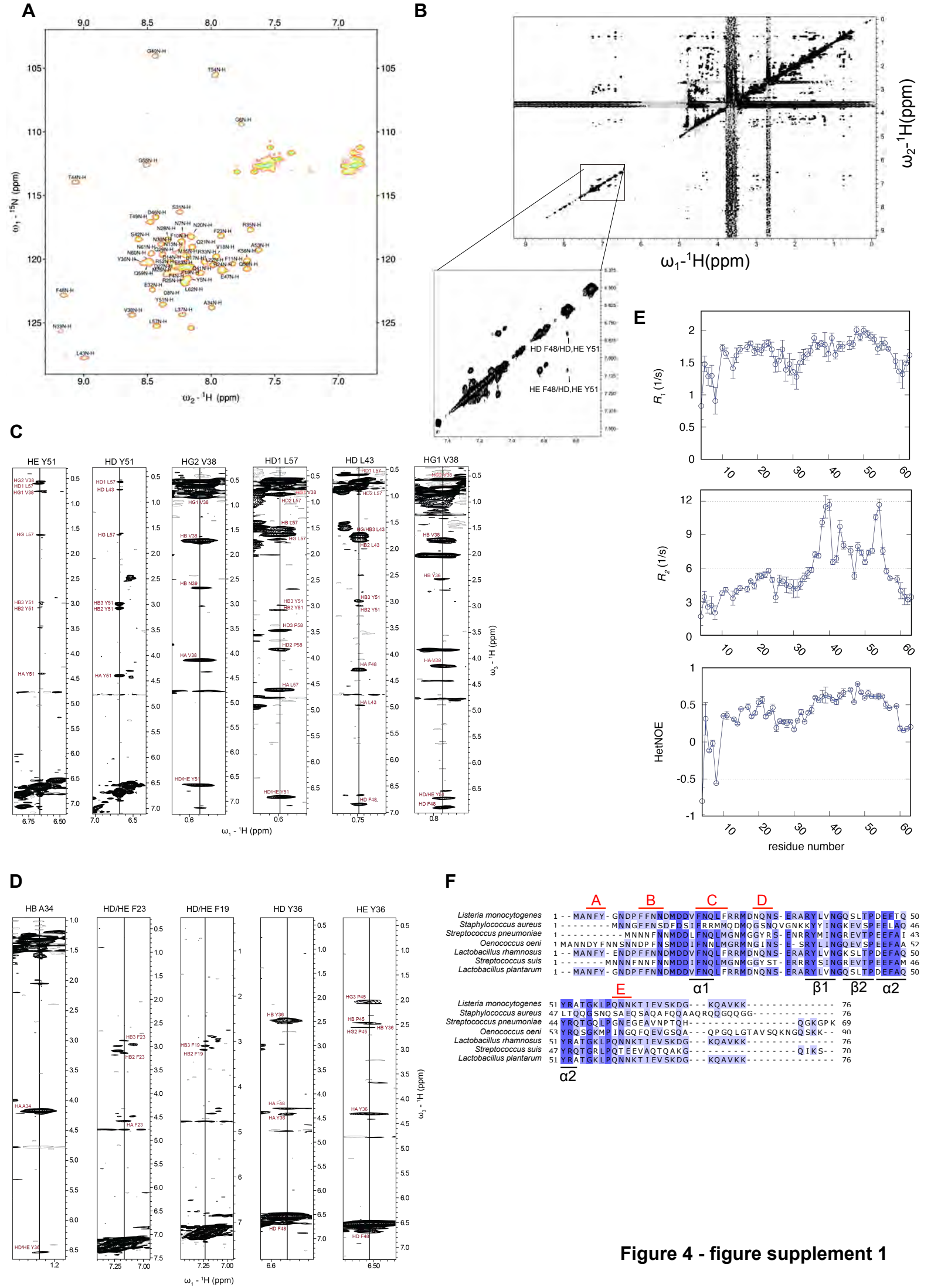

Figure 4 - figure supplement 1

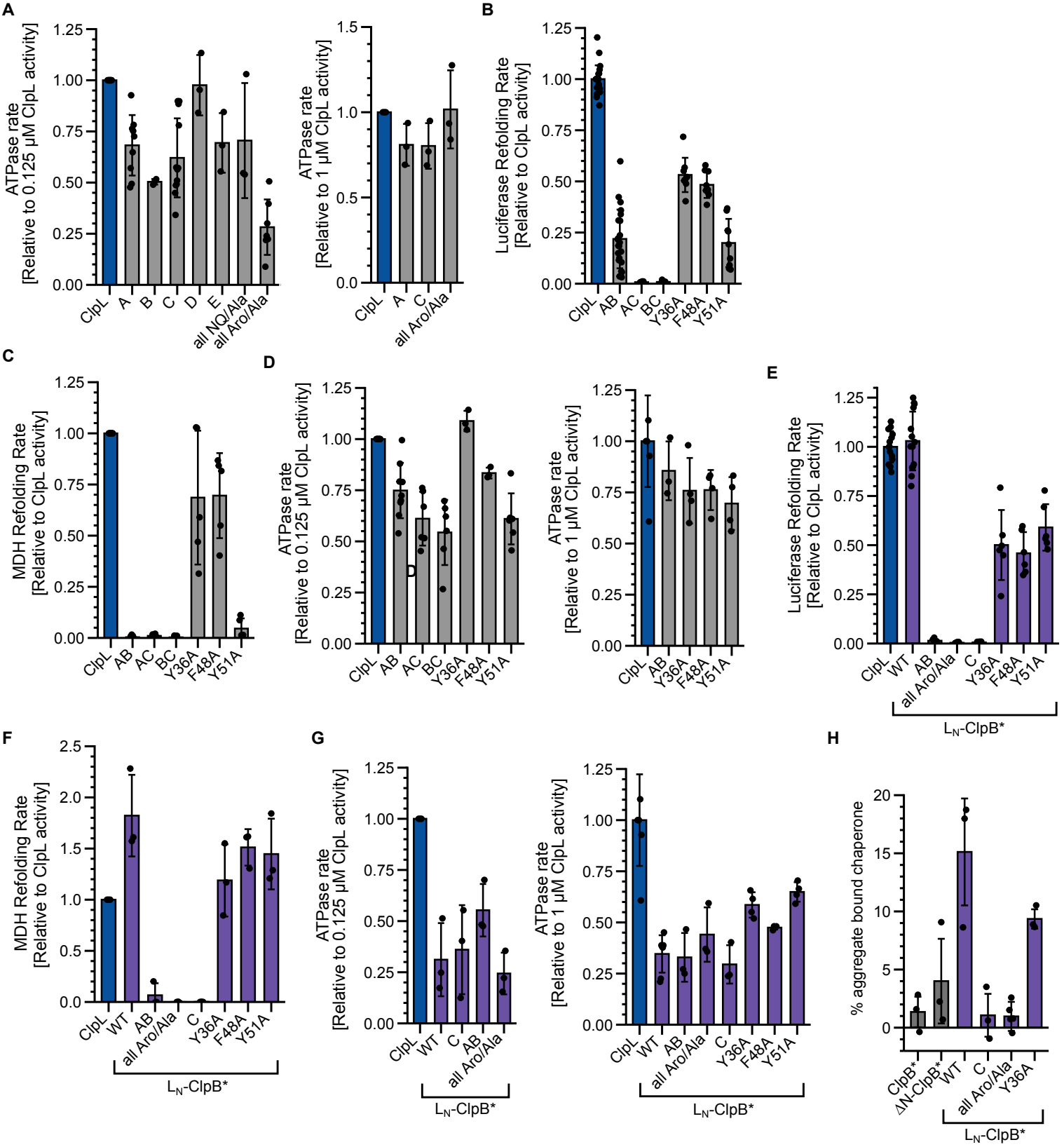

Figure 4 - figure supplement 2

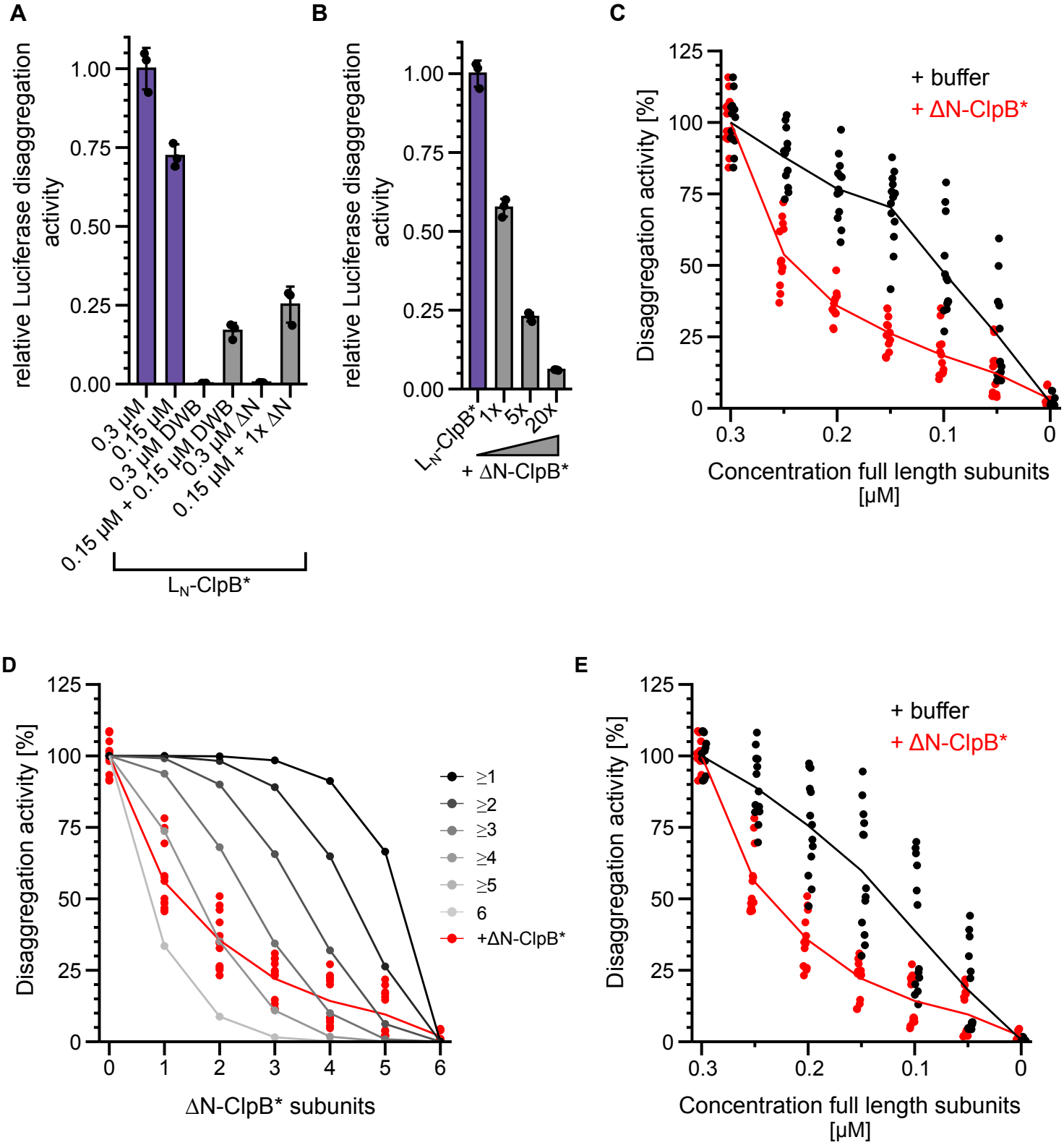

Figure 5 - figure supplement 1

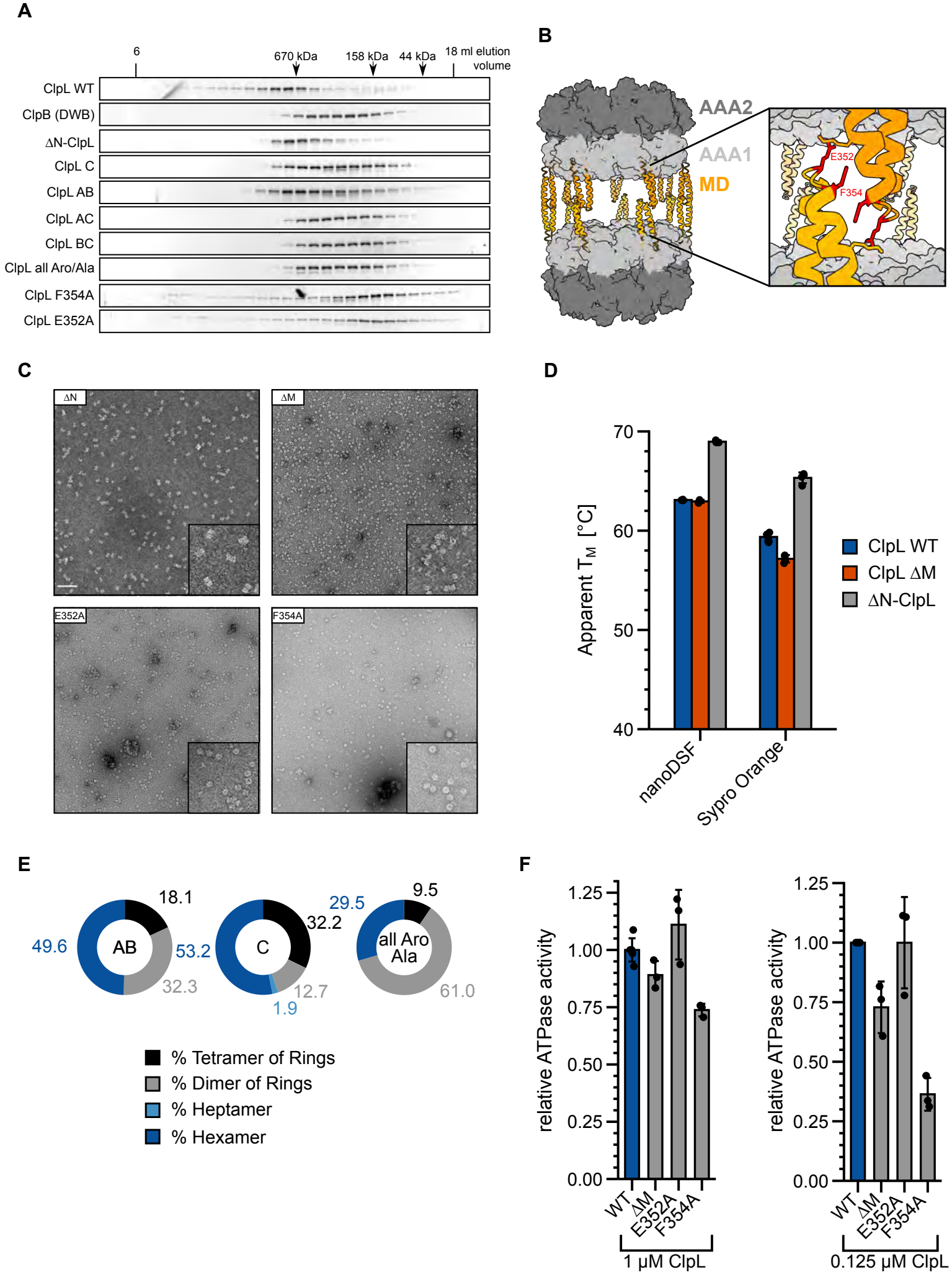

Figure 6 - figure supplement 1

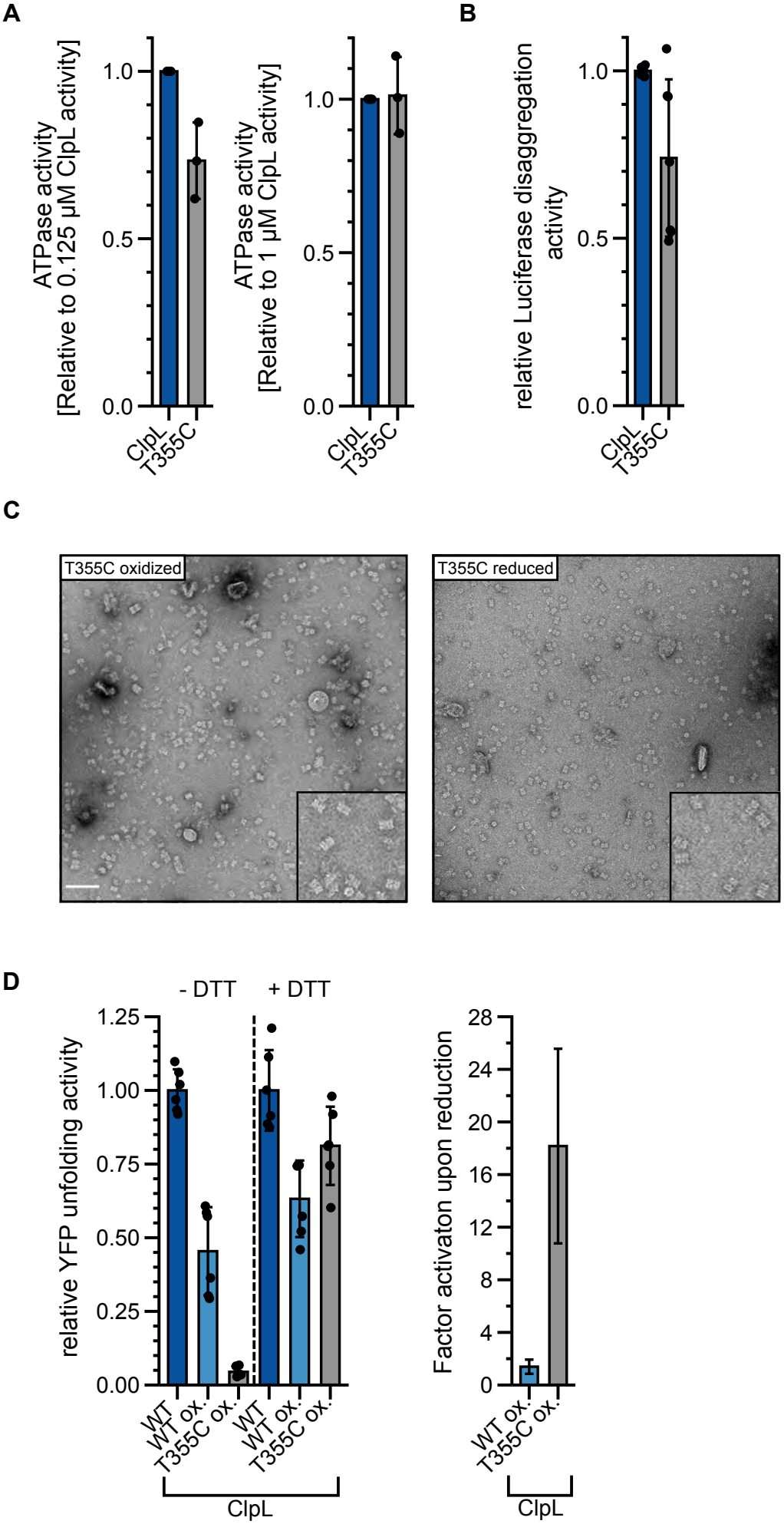

Figure 6 - figure supplement 2

Supplementary figure legends

Figure 1 – supplement figure 1
Sequence alignment of *Escherichia coli* ClpB, *Staphylococcus aureus* ClpC, *Pseudomonas aeruginosa* $ClpG_{GI}$ and *Listeria monocytogenes* ClpL. The domain organization is indicated. Similar and identical residues are highlighted in light and dark blue.

Figure 1 – supplement figure 2
ClpL is a potent, stand-alone disaggregase. (A) Disaggregation of aggregated Luciferase was monitored by turbidity measurements in presence of indicated chaperones. KJE: DnaK/DnaJ/GrpE. Initial turbidity was set at 100%. (B) Relative Luciferase disaggregation activities (% turbidity/min) were determined for indicated chaperone combinations. The disaggregation activity of ClpL was set to 1. (C) α-Glucosidase disaggregation activities (% turbidity/min) were determined in presence of indicated chaperones. Initial turbidity of α-Glucosidase aggregates was set to 100%. Disaggregation activity of ClpL was set to 1. (D) Left: MDH disaggregation activity of ClpL (% refolded MDH/min). Right: MDH disaggregation activities of indicated chaperones were determined. The activity of ClpL was set to 1. (E) Disaggregation activities of indicated chaperone combinations towards aggregated Luciferase, MDH, GFP and α-Glucosidase were determined. The activity of ClpL was set to 1. n.d.: not determined. Standard deviations are based on at least three independent experiments (B-E).

Figure 3 – supplement figure 1
ClpL disaggregation activity relies on ATP-fueled substrate threading. (A) Domain organization of ClpL. Pore loop (Y170, Y504) and Walker B (E197, E530) residues of AAA1 and AAA2 domains are indicated. (B) ClpL ATPase activities were determined at 0.125 and 1 μM protein concentrations. (C) ATPase activities of ClpL WT and indicated mutants were determined at 1 μM protein concentration. The ATPase activity of ClpL WT was set to 1. (D) Luciferase disaggregation activities (% refolded Luciferase/min) of ClpL WT and indicated mutants were determined. The activity of ClpL WT was set to 1. Standard deviations are based on at least three independent experiments (B-E).

Figure 3 – supplement figure 2
The ClpL NTD is crucial for disaggregation activity. (A) *E. coli dnaK103* cells harboring plasmids for IPTG-controlled expression of indicated disaggregases were grown at 30°C to mid-logarithmic growth phase and shifted to 49°C. Serial dilutions of cells were prepared at indicated time points, spotted on LB plates and incubated at 30°C. 100/500: μM IPTG added to induce disaggregase expression. p: empty vector control. (B-C) Production levels of disaggregases (ClpB, DnaK, ClpG, ClpL, ClpL-ΔN) in *E. coli ΔclpB* (B) and *dnaK103* (C) mutant cells. Cells were were grown at 30°C for 1.5 h and disaggregase expression was induced by addition of indicated IPTG concentrations (μM) for 2 h. Total cell extracts were prepared and levels of disaggregases were determined SDS-PAGE followed by Coomassie-staining. ClpL levels were additionally determined by western blot analysis using ClpL-specific antibodies. *p*: empty vector control.

Figure 4 – supplement figure 1
Structural analysis of ClpL NTD. (A) $^{1}H,^{15}N$-HSQC of ClpL NTD with resonance assignment labeled at each peak. Several residues exhibit dispersed peak position, indicative of folding. (B) $^{1}H,^{1}H$-2D NOESY in D_2O of ClpL NTD confirming NOEs between aromatic ring protons of the hydrophobic core formed by α2 and the β-sheet. NOEs of the second predicted core between α1 and α2 are absent, indicating that there is no interaction between α1 and α2. (C) Selected

strips of the ^{13}C-edited 3D NOESY-HSQC to illustrate that the predicted hydrophobic core between α2 and the β-sheet is present. Multiple cross-peaks (NOEs) are present between relevant residues (Y36, V38, L43, F48, Y51). (D) Selected strips of the ^{13}C-edited 3D NOESY-HSQC illustrating the absence of NOEs expected to between residues of the second hydrophobic core between α1 and α2. For these residues (F19, F23, A34, Y36) only intra-residue or sequential NOEs are visible (except for Y36, which has NOEs to residues of the first hydrophobic core). Thus, despite transient formation of the α1-helix, there is no or only transient interactions between α1 and α2. (E) ^{15}N spin relaxation data of ClpL NTD. Top: Longitudinal relaxation rates, middle: transverse relaxation rates, bottom: Heteronuclear NOEs. All three measurements show that the N-terminal region up to residue R35 is highly flexible, whereas the region of the hydrophobic core between α2 and the β-sheet higher heteronuclear NOE values and longer transverse relaxation rates indicating a higher degree of order. The altogether low heteronuclear NOE values, rarely above 0.6 indicate that the secondary structure elements (α1 vs. α2/β-sheet) are mobile with respect to each other in the ps-ns time scale. (F) Sequence alignment of ClpL NTDs. Similar and identical residues are highlighted in light and dark blue. The positions of secondary structural elements and of patches (A-E) composed of Y, F, N and Q residues are indicated.

Figure 4 – supplement figure 2

Mutant analysis of ClpL NTD. (A/D) ATPase activities of indicated ClpL mutants determined at 0.125 and 1 μM protein concentration. The ATPase activities of ClpL WT were set to 1. (B/C) Luciferase and MDH disaggregation activities (% refolded enzyme/min) of ClpL WT and indicated mutants were determined. The disaggregation activity of ClpL WT was set to 1. (E/F) Luciferase and MDH disaggregation activities (% refolded enzyme/min) of ClpL WT, L_N-ClpB* and L_N-ClpB* mutants were determined. The disaggregation activity of ClpL WT was set to 1. (G) ATPase activities of ClpL WT, L_N-ClpB* and L_N-ClpB* mutants were determined at 0.125 and 1 μM protein concentration. The disaggregation activity of ClpL WT was set to 1.

Figure 5 – supplement figure 1

Multiple ClpL NTDs are required for disaggregation activity. (A) Luciferase disaggregation activities of indicated L_N-ClpB* disaggregase mixtures were determined (DWB: ATPase deficient L_N-ClpB*-E279A/E678A, ΔN: ΔN -ClpB*). Protein concentrations (μM) are indicated. The disaggregation activity of 0.3 μM L_N-ClpB* was set to 1. (B) Luciferase disaggregation activities of L_N-ClpB* were determined in absence and presence of ΔN-ClpB* excess as indicated. The disaggregation activity of L_N-ClpB* was set to 1. (C) Luciferase disaggregation activities (% refolded Luciferase/min) were determined for mixtures of L_N-ClpB* and ΔN-ClpB* and were set as 100% for non-mixed L_N-ClpB* (0.3 μM). Mixing ratios are indicated as final concentration of L_N-ClpB* in 0.3 μM mixed hexamers. As control disaggregation activities of lower L_N-ClpB* concentrations were determined (+ buffer). (D) Luciferase disaggregation activities (% refolded Luciferase after 120 min) of mixed L_N-ClpB*/ΔN-ClpB* hexamers were determined and compared with curves calculated from a model (black to grey), which assumes that a mixed hexamer only displays disaggregation activity if it contains the number of NTDs indicated. Mixing ratios are indicated as number of ΔN-ClpB* in a hexamer. (E) Luciferase disaggregation activities (% refolded Luciferase after 120 min) were determined for mixtures of L_N-ClpB* and ΔN-ClpB* and were set as 100% for non-mixed L_N-ClpB* (0.3 μM). Mixing ratios are indicated as final concentration of L_N-ClpB* in 0.3 μM mixed hexamers. As control disaggregation activities of lower L_N-ClpB* concentrations were determined (+ buffer).

Figure 6 – supplement figure 1

ClpL rings interact in a M-domain dependent manner. (A) Oligomeric states of ClpL WT and indicated mutants were determined in presence of ATP by size exclusion chromatography. ATPase-deficient ClpB-E279A/E678A (DWB) served as reference for hexameric rings. Elution fractions were analyzed by SDS-PAGE. Positions of peak fractions of a protein standard are indicated. (B) Model of *Lm* ClpL highlighting the residues E352 and F354, which are crucial for M-domain mediated ring interactions. (C) Negative stain EM of indicated ClpL mutants. The insets show a magnification of a representative grid area. The scale bar is 100 nm. (D) Melting temperatures (T_M) of ClpL WT and indicated deletion mutants were determined in presence of ATPγS by nanoDSF or SYPRO®Orange binding. (E) Populations of diverse ClpL assembly states were determined based on 2D class averages for indicated ClpL mutants. (F) ATPase activities of indicated ClpL M-domain mutants were determined at 0.125 and 1 μM protein concentration. The ATPase activities of ClpL WT were set to 1. Standard deviations are based on at least three independent experiments (D/F).

Figure 6 – supplement figure 2

Stabilizing ClpL ring dimers by disulfide crosslinking. (A) ATPase activities of indicated ClpL WT and T355C were determined at 0.125 and 1 μM protein concentration. The ATPase activities of ClpL WT were set to 1. (B) Luciferase disaggregation activities (% refolded enzyme/min) of ClpL WT and T355C were determined. The disaggregation activity of ClpL WT was set to 1. (C) Negative stain EM of ClpL T355C in oxidized and reduced states in presence of ATP. The insets show a magnification of a representative grid area. The scale bar is 100 nm. (D) YFP unfolding rates (% YFP fluorescence/min) during disaggregation of aggregated Luciferase-YFP by ClpL WT and oxidized ClpL WT or ClpL T355C were determined in absence of DTT (-DTT). Oxidized variants (WT and T355C) were additionally preincubated with 10 mM DTT for 30 min and tested for YFP unfolding activity in presence of DTT (+DTT). The factor of increase in YFP unfolding activity upon reduction (+DTT) is indicated (right). Standard deviations are based on at least three independent experiments (A/B/D), standard deviations for the activity gain factors have been propagated from disaggregation activity standard deviations.